Design and synthesis of novel anticancer and antifibrosis compounds

THESIS

Submitted for partial fulfillment of the requirement for the degree of Doctor of Philosophy in Pharmaceutical Sciences

By

Ahmed Khairy Hamdy Edris

(*MSc, BSc*)

PhD student, Department of Medicinal and biological Chemistry,

Graduate School of Pharmaceutical Sciences,

Kumamoto University, Japan

March 2023

Design and synthesis of novel anticancer and antifibrosis compounds

Ahmed Khairy Hamdy Edris

Department of Medicinal and Biological Chemistry, Graduate School of Pharmaceutical Sciences, Kumamoto University

Millions of individuals die each year from the two great global burdens of cancer and fibrosis. Our goal, as outlined in chapter1 &2, is to design and synthesize novel promising lead compounds that can be turned into potential treatments for cancer and fibrosis.

Chapter 1. Isatin-based anticancer derivatives

Isatin is a privileged scaffold in the field of medicinal chemistry and drug discovery due to its broad range of biological actions like anti-cancer, anti-bacterial, antifungal, anti-diabetic, anti-convulsant, anti-tubercular, anti-HIV, neuroprotective, antioxidant, anti-glycation, anti-malarial, anti-inflammatory, analgesic, and anti-anxiety. The great scientific research in development of isatin-based anticancer drugs accomplished with discovery of sunitinib which was approved for treatment of gastrointestinal stromal tumor and renal cell carcinoma. α,β-Unsaturated ketone scaffold is a common structural feature in many natural and synthetic compounds including the chemo-preventive agent; curcumin which displayed anticancer activity. Inspired by the structure features of approved isatin-based anticancer drugs and α,β-unsaturated ketone, herein novel compounds combining both structural features of isatin-based anticancer drugs with α,β-unsaturated ketone were synthesized. The synthesized compounds were screened against sixty cancer cell lines in single dose assay (10 μM) according to NCI protocol. All compounds revealed promising cytotoxic activity against numerous cancer cell lines. Acute myeloid leukemia (HL-60) cell line was among the most sensitive cell lines in NCI one dose assay. Therefore, *in vitro* five doses antiproliferative assay of the synthesized compounds **5a-h** against HL-60 cells was conducted and explored that the compounds **5b** and **5g** are the most potent with submicromolar IC_{50} values. Moreover, **5b** and **5g** induced apoptosis and revealed the ability to arrest cell cycle progression at G1 phase. Additionally, **5b** and **5g** demonstrated inhibitory activity on ERK1/2 phosphorylation in HL-60 cells, and this effect may be responsible for its subsequent actions on apoptosis and cell cycle distribution. *In silico* studies demonstrated binding of **5b** and **5g** to ERK active site in the same manner as the potent ERK1/2 inhibitor co-crystallized ligand SCH772984, in addition to the favorable pharmacokinetics for the synthesized compounds **5a-h**.

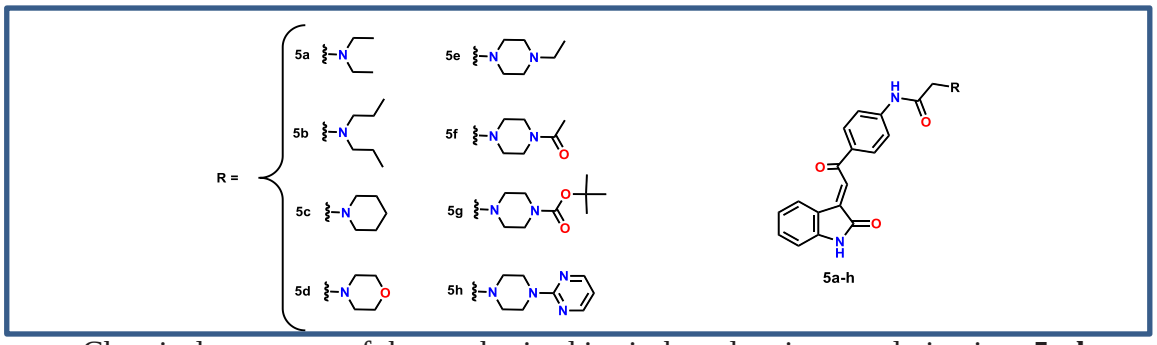

Chemical structures of the synthesized isatin-based anticancer derivatives **5a-h**

Chapter 2. 5-chlorosalicylamide and 2-amino-5-phenylthiophen-3-carboxamide derivatives

Fibrosis is defined by the excessive accumulation of the extracellular matrix (ECM), such as collagen and fibronectin, in and around inflamed or damaged tissue, which can result in permanent scarring, organ malfunction and, subsequently death. 5-Chlorosalicylamide derivative like niclosamide was reported to be effective in treatment of idiopathic pulmonary fibrosis through blocking PI3K-mTORC1 signaling pathway. Additionally, the 2-amino-5-phenylthiophen-3-carboxamide derivatives were found to be effective in inhibition of NF-kB which is involved in pathogenesis of pulmonary fibrosis. Motivated by the previous finding and our group's interest in development of antifibrotic drugs, I designed and synthesized novel 5-chlorosalicylamide and 2-amino-5-phenylthiophen-3-carboxamide derivatives and tested their antifibrosis activity through measurement of their effect on collagen production in a line of healthy human dermal fibroblasts. The antifibrosis assay was conducted using a positive control HPH-15, which was developed by our group as promising preclinical antifibrotic drug for skin fibrosis. In one hand, 5-chlorosalicylamide derivatives indicated a substantial suppression of collagen formation even more than HPH-15, but unfortunately, it showed cytotoxicity. On the other hand, 2-amino-5-phenylthiophen-3-carboxamide derivative **17b** elucidated promising collagen production inhibitory results that is comparable to HPH-15.

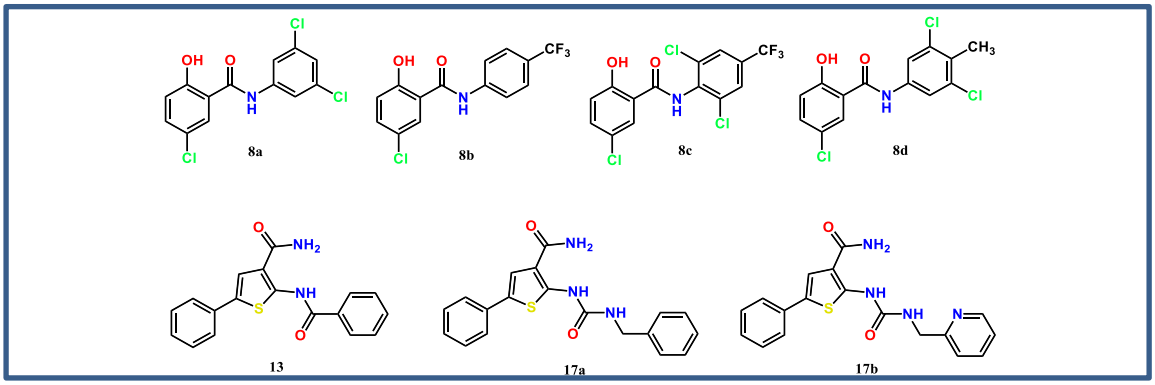

Chemical structures of the synthesized 5-chlorosalicylammide and 2-amino-5-phenyl-3-carboxamide derivatives **8a-d**, **13** and **17a,b**

Reference articles

Ahmed K. Hamdy, *Takashi Sakamoto, Tsugumasa Toma, Masaharu Sakamoto, Mohammed A. S. Abourehab, Masami Otsuka, Mikako Fujita, Hiroshi Tateishi and Mohamed O. Radwan.* "New Insights into the Structural Requirements of Isatin-derived Pro-apoptotic Agents against Acute Myeloid Leukemia". *Pharmaceuticals, 2022, 15, 1579.*

Ciftci, Halil I., Mohamed O. Radwan, Belgin Sever, ***Ahmed K. Hamdy****, Safiye Emirdağ, N. Gokce Ulusoy, Ece Sozer et al.* "EGFR-targeted pentacyclic triterpene analogues for glioma therapy." *International Journal of Molecular Sciences 22, no. 20 (2021): 10945.*

Abdel El-wahab, Hend AA, ***Ahmed K. Hamdy****, Carola Schulzke, Tarek Aboul-Fadl, and Wesam S. Qayed.* "Crystal structure and quantum chemical calculations of (E) 1-benzyl-3-((4-methoxyphenyl) imino)-5-methylindolin-2-one." *Journal of Heterocyclic Chemistry 58, no. 8 (2021): 1601-1609.*

Acknowledgement

Firstly, prayerful thanks to our merciful **ALLAH**, who gives me everything I have.

Words are not enough to express my thanks to **Prof. Dr. Masami Otsuka** for accepting me to be a member inside his research group, his excellent supervision, patience and valuable guidance during my PhD study. He motivated me to think independently and scientifically, which has been very beneficial for my career progress.

I am greatly honored to convey my real appreciation and thanks to **Prof. Dr. Mikako Fujita** for her dear supervision and provision in most biological assays of my thesis as well as her valuable discussion and precise revision. She always gives me her sincere advice and help to accomplish this work. Her comments and assistance were very supporting to me. I am very lucky to have the great opportunity to be a member in her research group.

I would like to express my sincere appreciation and gratitude to **Dr. Mohamed O. Radwan** for his keen supervision, reviewing the manuscript with a great care and precision, valuable advices and for his great support for me during my PhD study.

I am very grateful to **Dr. Hiroshi Tateishi** for his continuous interest, helpful ideas, his fruitful comments and for his great help in biological assays.

I am especially grateful for my dissertation committee members including **Prof. Dr. Makoto Nakajima, Prof. Dr. Shunsuke Kotani and Prof. Dr. Yoshihiri Kobashigawa**, who spend their priceless time and effort to evaluate my work.

I am thankful to all of the past and present members of Prof. Dr. Otsuka laboratory who have been like my family during my PhD study, supporting me personally and scientifically.

My special thanks for the Egyptian Ministry of Higher Education, Mission Sector for supporting and funding me through Egypt-Japan Education Partnership (**EJEP**).

Last but not least, I would like to express my sincere thanks to, my wife, my parents, and my kids for their emotional support and much effort. To everyone who made this work possible, thank you very much.

Dedication

With all love this work is dedicated to:

My Wife, My Parents and My Beautiful kids;

Yousef & Kenda

List of Abbreviations

Abb.	The word
ACEIs	Angiotensin Converting Enzyme Inhibitors
ATI	Angiotensin I
ALL	Acute Lymphoid Leukemia
AML	Acute Myeloid Leukemia
ATP	Adenosine Triphosphate
BOILED-Egg	Brain Or IntestinaL EstimateD permeation method
CDK	Cyclin-Dependent Kinase
CLL	Chronic Lymphoid Leukemia
CML	Chronic Myeloid Leukemia
CNS	Central Nervous System
CRC	Colorectal Cancer
CTGF	Connective Tissue Growth Factor
CVD	Cardiovascular Disease
DCM	Dichloromethane
DIPEA	Diisopropylethylamine
DMF	Dimethylformamide
DMSO	Dimethyl sulfoxide
DNA	Deoxyribonucleic acid
DTP	Developmental Therapeutics Program
EBV	Epstein-Barr virus
ECM	Extracellular Matrix
EtOH	Ethanol
ERK1/2	Extracellular Signal-related Kinases 1 and 2
FAB	Fast Atom Bombardment
FBS	Fetal Bovine Serum
FDA	Food and Drug Administration
GI%	Growth Inhibition%
GIST	Gastrointestinal Stromal tumor
HCV	Hepatitis C Virus
HIV	Human Immunodeficiency Virus
HPH-15	Histidine-Pyridine-Histidine-15
HPV	Human Papillomavirus
HRMS	High Resolution Mass Spectroscopy
IC_{50}	50% Inhibitory Concentration

IL	Interleukin
KSHV	Kaposi's Sarcoma-associated Herpesvirus
Kcal/mol	Kilocalorie/mole
Lys	Lysine
MAPK	Mitogen-Activated Protein Kinase
Met	Methionine
MOE	Molecular Operating Environment
MTT	3-(4, 5-Dimethylthiazolyl-2)-2, 5-diphenyltetrazolium bromide
NASH	Nonalcoholic Steatohepatitis
NCI	National Cancer Institute
NF-κ B	Nuclear factor kappa-light-chain enhancer of activated B cells
NMR	Nuclear Magnetic Resonance
PDB	Protein Data Bank
p-ERK1/2	Phosphorylated-Extracellular Signal-related Kinases 1 and 2
Pi3K	Phosphoinositide-3-kinase
PLC	Phospholipase C
RAS	Rat Sarcoma
RCC	Renal Cell Carcinoma
RNA	Ribonucleic Acid
RTKs	Receptor Tyrosine Kinases
RTKIs	Receptor Tyrosine Kinase Inhibitors
SI	Selectivity Index
α-SMA	α-Smooth Muscle Actin
SSc	Systemic Sclerosis
STAT3	Signal transducer and activator of transcription 3
TGF-β	Transforming growth factor-β
THF	Tetrahydrofuran
Tyr	Tyrosine

Table of Contents:

General Introduction

I. Cancer

a. Cancer definition

Cancer remains a global health concern, as it is the second leading cause of death in the world after cardiovascular diseases. Therefore, it is a critical global burden that threatens millions of people worldwide. Cancer is a genetic disease and developed as a result of alterations in oncogenes, tumor-suppressor genes, and microRNA genes [1]. It starts when body normal cells start growing uncontrollably producing invasive and nonfunctioning cells. Cancer cells can invade nearby tissues or even migrate to distant organs through blood circulation or lymph vessels; this spreading is called metastasis which sophisticates cancer treatment [2].

b. Cancer causes

Generally, cancer cells develop from normal cells due to damage of DNA which cannot be repaired. This DNA damage may be inherited genetic defects from patient's parents, or it may result from exposure to physical, chemical or biological carcinogens [3]:

1) Physical Carcinogens:

Ionizing radiation such as radon, ultraviolet rays from sunlight, uranium, radiation from alpha, gamma, beta, and X-ray-emitting sources [3].

2) Chemical Carcinogens:

Compounds like cadmium, silica, nitrosamines, asbestos, benzene, vinyl chloride, nickel, and benzidine. Moreover, tobacco consumption is a major

cause of cancer as it contains about 60 known potent cancer-causing toxins or chemicals [4].

3) Biological Carcinogens:

Biological carcinogens like infections from certain bacteria, viruses, or parasites and pathogens like hepatitis B and C, human papillomavirus (HPV), EBV or Epstein-Barr virus, Kaposi's sarcoma-associated herpesvirus (KSHV), Markel cell polyomavirus, Schistosoma, and helicobacter pylori [3].

c. Cancer types [3]

Cancers are divided into various types that are:

i. Carcinomas:

It begins in the tissue or the skin, which covers the glands and internal organ surface. It forms a solid tumor such as lung cancer, breast cancer, prostate cancer and colorectal cancer.

ii. Sarcomas:

It starts in the tissues which connect and support the body such as nerves, tendons, joints, bone, muscles, blood vessels, and lymph vessels.

iii. Leukemias:

Leukemia is a cancer of the blood which begins when healthy blood cells grow uncontrollably and change. It is divided into 4 subtypes, that are acute myeloid leukemia (AML), acute lymphocytic leukemia (ALL), chronic myeloid leukemia (CML), and chronic lymphocytic leukemia (CLL).

iv. Lymphomas:

Lymphoma is cancer that begins in the lymphatic system such as Hodgkin lymphoma and non-Hodgkin lymphoma.

v. Central Nervous System Cancers:

Cancer that starts in brain tissues and spinal cord such as CNS lymphomas, vestibular schwannomas, gliomas, pituitary adenomas, primitive neuro-ectodermal tumors, meningiomas, and vestibular schwannomas.

vi. Multiple Myeloma:

Multiple myeloma is cancer that begins in plasma cells, another type of immune cell. The myeloma cells which are plasma cells, are build up in bone marrow and make tumors in bones. It is called plasma cell myeloma and Kahler disease.

vii. Melanoma:

It starts in melanocytes, cells that make melanin, i.e., the pigment that gives the color to the skin. Mainly melanomas develop on the skin, but it can also develop in other pigmented tissue like an eye.

d. Cancer treatment

There are various types of cancer treatments, which depend upon the cancer type and how to advance it is. Some patients have only one cancer treatment but mainly have a combination of treatments like surgery with radiation therapy.

1. Surgery:

Surgery prevents or reduces cancer spread and removes it from the body. Surgeries are used for the solid tumor, which is located in one area and cannot be used for metastatic cancer or leukemia i.e., blood cancer [3].

2. Radiotherapy:

In radiotherapy high doses of radiation are used to treat cancer by shrinking tumors, killing cancer cells, and slow the growth of cancer cells by damaging their DNA. The damaged DNA does not repair, and the dead cells

are removed by the body. Radiation therapy is given with other cancer treatments for better results such as chemotherapy, surgery, and immunotherapy [3].

3. Chemotherapy:

Chemotherapy was first developed at the beginning of the 20th century with discovery of efficacy of nitrogen mustard in treatment of non-Hodgkin's lymphoma. Nitrogen mustard is an alkylating agent which acts through alkylation of DNA, RNA and proteins inside cancer cells. In 1948, the folate antagonist methotrexate was first used for treatment of leukemia in children. Methotrexate is an antimetabolite folic acid antagonist which act through inhibition of DNA synthesis. Other antimetabolite anticancer drugs were then developed such as 6-mercaptopurine and 5-fluorouracil. In the 1950s, Eli Lilly natural products group announced that plant alkaloids extracted from *Vinca rosea* such as vincristine were beneficial to leukemia patients. Vinca alkaloids (vincristine and vinblastine) act in the same way as paclitaxel through inhibition of microtubules and cell mitosis. The great efforts in the field of chemotherapy drug discovery were accomplished with discovery of several anticancer drugs such as anticancer antibiotics, hormones, receptor tyrosine kinase inhibitors (RTKIs) and cyclin dependent kinase (CDK) inhibitors [5], **(Figure 1)**.

RTKIs inhibit receptor tyrosine kinases (RTKs) which are key regulatory signaling proteins governing cancer cell growth and metastasis. During the last two decades, several RTKIs were developed and used as the first- or second-line therapy in different types of cancer. Activation of RTKs activate in turn three main intracellular kinases: phosphoinositide 3-kinase (PI3K), rat sarcoma (RAS), and phospholipase C (PLC). Subsequently, activation of RAS results in activation of RAS-RAF-MEK-ERK signaling cascade (Mitogen activated protein kinase; MAPK pathway) [6].

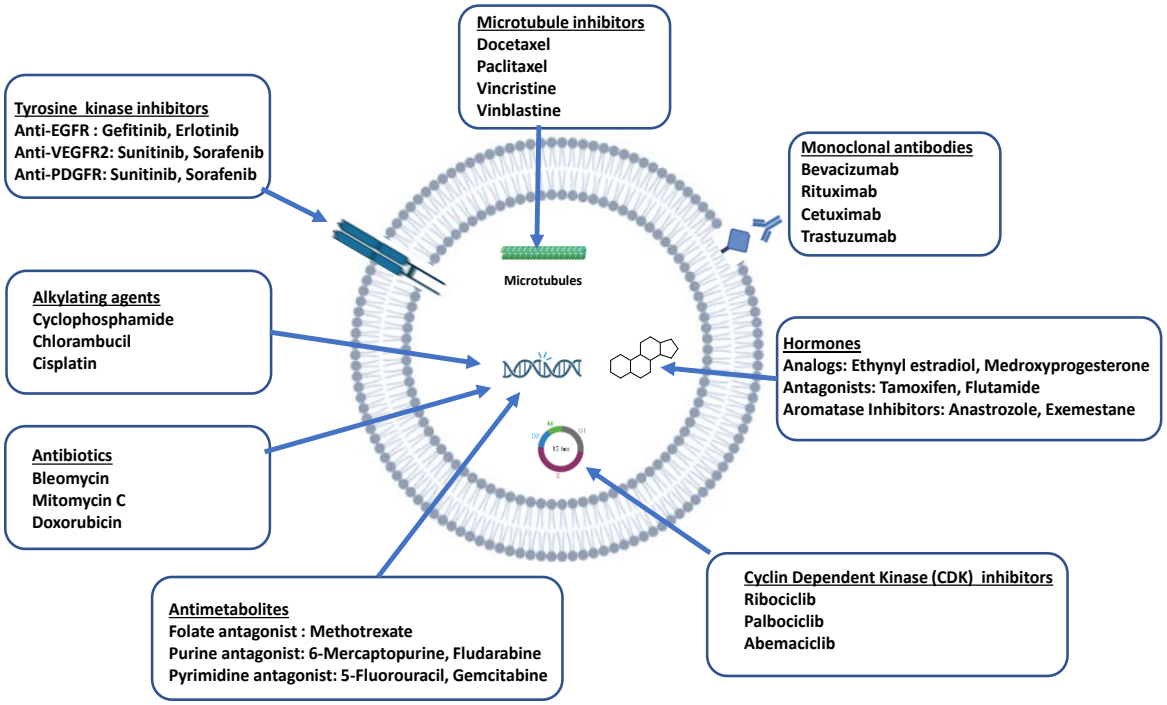

Figure 1: Different approved anticancer drugs

RAS-RAF-MEK-ERK signaling cascade (MAPK pathway) mediates cell proliferation through signal transduction from cell surface (RTKs) to transcription factors inside nucleus. Stimulation of RTK by mitogens, growth factors and cytokines recruits and activates RAS which in turn activates Raf family (A-Raf, B-Raf and C-Raf). Active Raf phosphorylates and activates the dual-specificity kinases MEK1 and its homologue MEK2 (MEK1/2) which sequentially phosphorylate the serine/threonine kinases, extracellular signal-related kinases 1 and 2, ERK1/2 [7]

Phosphorylated ERK1/2 (p-ERK1/2) catalyze and phosphorylate 250 cytosolic and nuclear downstream substrates including transcription factors (e.g., Ets-1, Elk-1, c-Fos, c-Jun), the RSK family of kinases, phosphatases, apoptotic proteins, and cytoskeletal proteins, among many others. This wide array of substrates regulates many cellular functions, such as gene transcription, cell cycle progression, proliferation, migration, adhesion, survival, and metabolism [8], **(Figure 2)**. Furthermore, it was reported the importance of

ERK1/2 for transition of cells from G1 to S phase in cell cycle and its ability to inhibit cell apoptosis through inhibition and phosphorylation of caspase 9 [9].

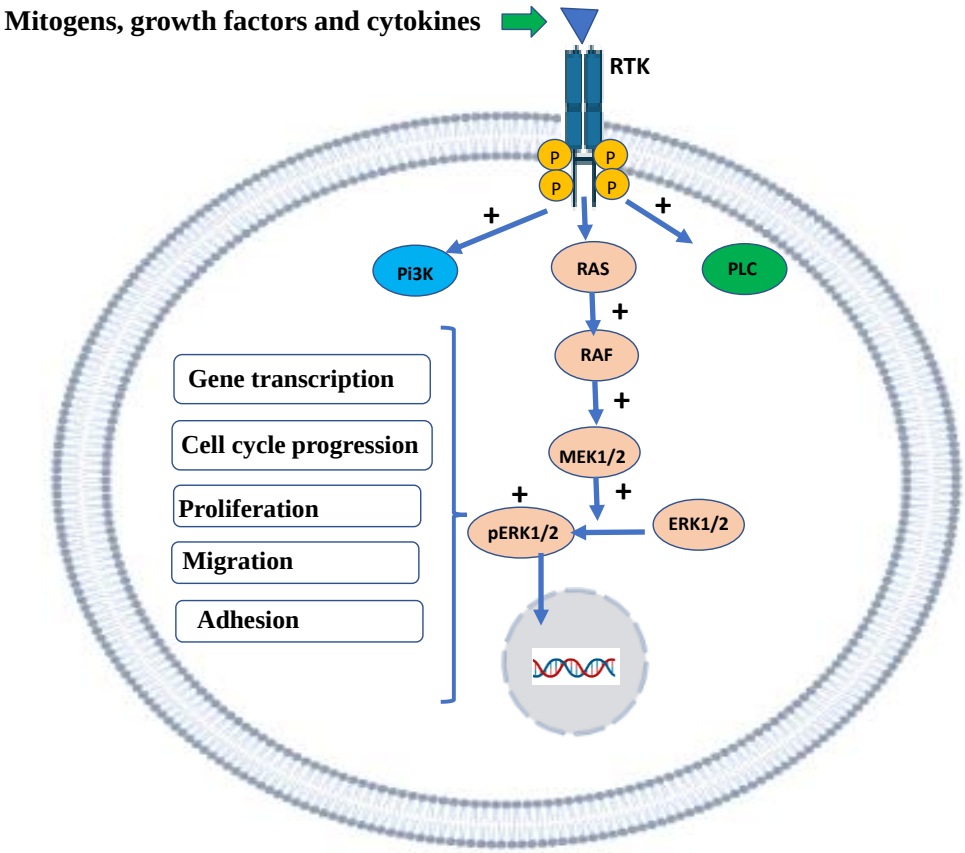

Figure 2: Activation of RTK and MAPK pathway

More than 30% of malignancies, including melanoma, lung, pancreatic, colorectal (CRC), and acute myeloid leukemia (AML), have RAS or RAF mutations, which activate the RAS-RAF-MEK-ERK signaling cascade (MAPK pathway) [10,11]. Trametinib and cobimetinib are two approved drugs on the market that inhibit MEK1/2 kinases, **(Figure 3)**. However, their therapeutic benefits are constrained by resistance brought on by MEK mutations that restore ERK activity. Location of ERK1/2 in the distal end of RAS-RAF-MEK-ERK pathway and because it is rarely undergone mutations makes ERK1/2 attractive target for development of anticancer drugs. Currently, design and synthesis of compounds with antitumor activity through targeting

ERK1/2 has increased and some of them entered clinical trials **(Figure 4)**, but no drug was approved till date [7,12].

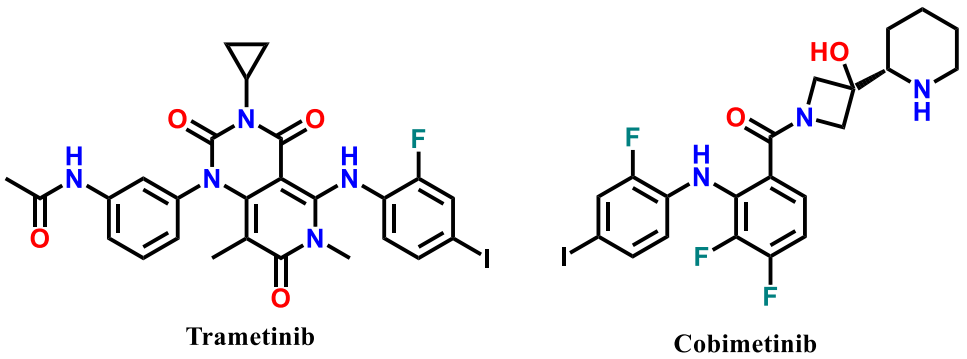

Figure 3: Chemical structures of MEK1/2 inhibitors as approved drugs

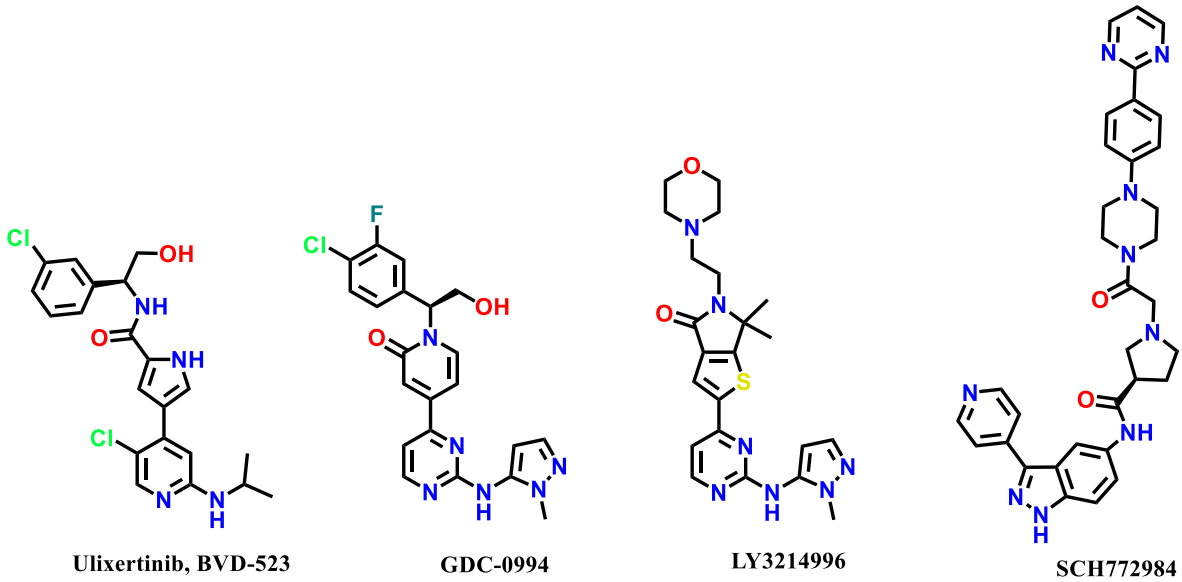

Figure 4: Chemical structures of ERK1/2 inhibitors used in clinical trials

II. Fibrosis

a. Definition of fibrosis

Fibrosis is defined by the excessive accumulation of the extracellular matrix (ECM), such as collagen and fibronectin, in and around inflamed or damaged tissue, which can result in permanent scarring, organ malfunction and, subsequently death as seen in end-stage idiopathic pulmonary fibrosis (IPF), liver disease, kidney disease, and heart failure. Fibrosis is also a major pathological feature of many chronic autoimmune diseases, including systemic sclerosis (scleroderma), rheumatoid arthritis, Crohn's disease, ulcerative colitis, myelofibrosis and systemic lupus erythematosus [13–15].

Numerous clinical outcomes, including tumor invasion and metastasis, chronic graft rejection, and the etiology of many progressive myopathies, are also influenced by fibrosis. Despite the fact that fibrosis is now understood to be a significant contributor to morbidity and death in the majority of chronic inflammatory diseases, there are few, if any, therapy options that particularly target the pathophysiology of fibrosis [14].

b. Causes of fibrosis

Progressive fibrotic disease can be brought on by many distinct triggers such as inherited genetic disorders, chronic infections (like the chronic hepatitis C virus [HCV] infection), excessive alcohol consumption, recurrent exposure to toxins, irritants or smoke, chronic autoimmune inflammation, minor human leukocyte antigen mismatches in transplants, myocardial infarction, high serum cholesterol, obesity, and poorly controlled diabetes and hypertension [14].

b. Types of fibrosis

As shown in **Figure 5**, fibrosis affects a variety of tissues and organs, occurring more commonly in the heart, lung, kidney, liver, and skin [16], and

less frequently in the pancreas, colon, eye [17], nervous system [18], joint and tendon among other tissues and organs (arthrofibrosis) [19].

1- Idiopathic pulmonary fibrosis (IPF)

IPF is a chronic and progressive interstitial lung disease of unknown etiology and with a poor prognosis. Adults in their middle and later years are more at risk for IPF [20]. The global incidence and prevalence of IPF are in the range of 0.09 and 1.30 per 10,000 people and increasing dramatically year by year. The United States, South Korea and Canada have the highest incidence of IPF within studied countries [21,22]. Histopathological characteristics of IPF revealed excessive deposition of ECM, resulting in deformation of normal pulmonary architecture and irreversible loss of lung function [23].

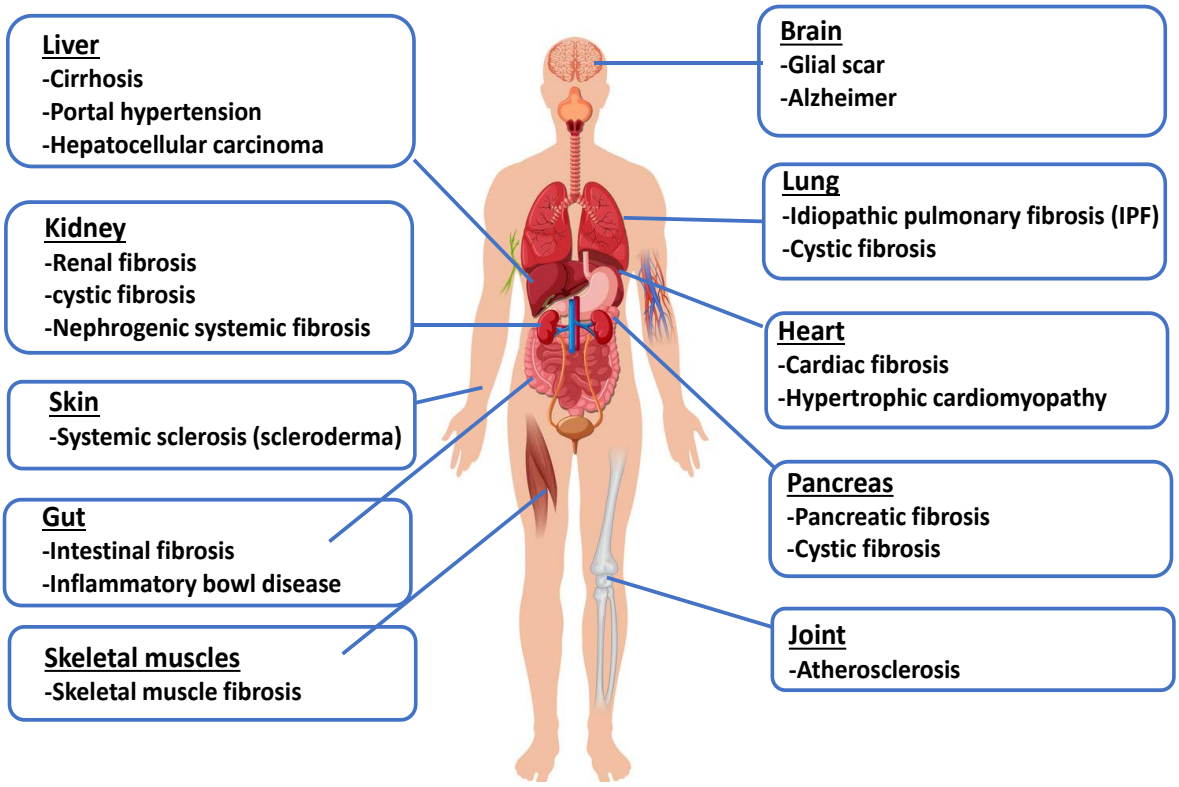

Figure 5: Fibrosis and related diseases in various tissues and organs.

Clinical signs of IPF include a worsening cough, progressive dyspnea, a considerable decline in lung compliance, and a reduced quality of life [22,24]. Two drugs, nintedanib and pirfenidone **(Figure 6)** have been approved for

treatment of IPF patients. While pirfenidone is an oral pyridin-2-one derivative with anti-inflammatory, antioxidant, and antifibrotic properties, nintedanib is an isatin-based tyrosine kinase inhibitor. These two medications have demonstrated a slowdown of disease development and a reduction in lung function deterioration [25].

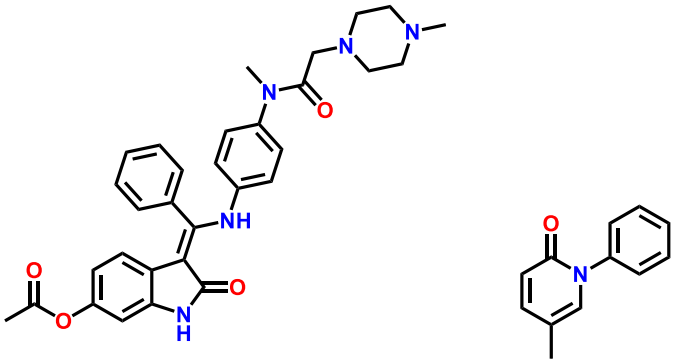

Figure 6: Chemical structures of drugs used in treatment of IPF

2- Liver fibrosis

Liver fibrosis results from exposure of the liver to chronic damage in conjunction with the accumulation of ECM proteins, which is a characteristic of the majority of chronic liver diseases [26]. In industrialized nations, persistent HCV infection, alcoholism, and nonalcoholic steatohepatitis (NASH) are the leading causes of liver fibrosis. The accumulation of ECM proteins causes cirrhosis by creating a fibrous scar on the liver, which deforms the hepatic architecture. Cirrhosis generates liver dysfunction and increases intrahepatic resistance to blood flow, which result in hepatic insufficiency and portal hypertension, respectively [27].

Pharmaceutical and biotechnology companies are very interested in development of antifibrotic drugs, and clinical trials are actively being conducted. However, hepatic fibrosis is currently not treatable with an effective therapeutic; instead, the causal factor must still be removed [28]. In experimental models of chronic liver injury, a number of drugs were found to

be able to decrease the formation of scar tissue. The most promising medications, despite their effectiveness has not been examined in humans, are those that block the renin-angiotensin system and antioxidants [13].

3. Heart fibrosis

Since cardiovascular disease (CVD) causes 31% of deaths worldwide, it continues to be the leading cause of mortality [29]. Endomyocardial fibrosis and ischemic heart disease are the primary causes of end-stage heart failure [30]. There is an urgent need to develop cutting-edge diagnostic techniques and improved therapies for cardiac fibrosis. Fibrosis is a well-recognized cause of morbidity and mortality [29]. The most frequent cause of fibrotic scarring in cardiac muscle is myocardial infarction, although there are numerous additional disorders that may encourage cardiac fibrosis, including hypertension, diabetic hypertrophic cardiomyopathy, and idiopathic dilated cardiomyopathy [31,32].

Cardiac fibrosis is a pathological ECM remodeling process that causes anomalies in matrix quality and composition as well as a reduction in the function of the heart muscle [31]. ECM deposition is initially a defensive process that can aid in tissue regeneration and wound healing. However, persistent and excessive ECM deposition, in particular the production of collagen type I, results in impaired tissue function [33].

Angiotensin converting enzyme inhibitors (ACEIs) and ATI receptor antagonist, β-blockers, endothelin antagonists, and statins are currently used treatments to affect the fibrotic response in injuries [34]. Additionally, eplerenone, which has been FDA-approved since 2002, has been developed as a medication that prevents the development of fibrosis by obstructing the aldosterone pathway [35]. There are also approaches to influence fibroblast activation by blocking TGF-β or Smad3 signaling; however, there is a need for implementing more targeted interventions [33,36].

4. Systemic sclerosis (scleroderma)

Scleroderma, also known as systemic sclerosis (SSc), is a systemic autoimmune disease of unknown etiology. It is characterized by early vascular injury and inflammation, followed by fibrosis of the skin and visceral organs [37]. The usual initial symptom of SSc is swelling then thickening and tightening of the skin at the ends of the fingers. Raynaud syndrome, in which the fingers suddenly and temporarily become very pale and tingle or become numb, painful, or both in response to cold or emotional upset, is also common. Fingers may become bluish or white. Heartburn, difficulty in swallowing, and shortness of breath are occasionally the first symptoms of systemic sclerosis. Aches and pains in several joints often accompany early symptoms. Sometimes inflammation of the muscles (myositis), with its accompanying muscle pain and weakness, develops .

The pathophysiological hallmark of SSc is the excessive deposition of collagen and other ECM components in the affected organs. Activated fibroblasts and α-smooth muscle actin (α-SMA)-positive myofibroblasts are largely responsible for excessive matrix synthesis and tissue deposition. Numerous profibrotic molecules, such as transforming growth factor (TGF), connective tissue growth factor (CTGF), platelet-derived growth factor, interleukin (IL)-4, IL-6, and IL-13, and endothelin-1, play a role in the complex chain of events that lead to fibroblast activation and myofibroblast transformation. It is widely recognized that TGFβ-/Smad signaling is important for the pathophysiology of SSc [37].

Till date there is no drug which can stop the progression of SSc. However, drugs can relieve some symptoms and reduce organ damage. In a mouse model of SSc, the histidine-pyridine-histidine ligand HPH-15 (**Figure 7**) developed by our group, reduces skin inflammation and consequent fibrosis by inhibiting TGF-β/Smad signaling and the fibrogenic activity of human skin

cells *in vitro*. In preclinical study, HPH-15 was shown to have a number of benefits, such as the fact that it is an orally active drug with a great safety profile and has the potential to be a candidate for SSc clinical trials [37,38].

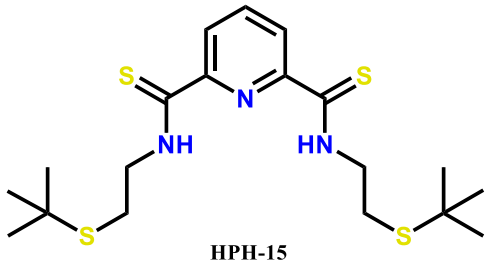

HPH-15

Figure 7: Chemical structure of HPH-15

Chapter (1)
Isatin-based anticancer derivatives

1.1 Introduction

1.1.1 About isatin

Erdmann and Laurent were the first to isolate isatin (1*H*-indole-2,3-dione) as an indigo oxidation byproduct using nitric acid and chromic acid. Additionally, it was discovered in human being as a metabolic byproduct of the hormone adrenaline. Additionally, many isatin derivatives are found naturally in plants [38]. Isatin and its derivatives demonstrate various biological activities like anti-cancer, anti-bacterial, antifungal, anti-diabetic, anti-convulsant, anti-tubercular, anti-HIV, neuroprotective [39], antioxidant [40], anti-glycation [41], anti-malarial [42], anti-inflammatory [43], analgesic [44], and anti-anxiety [45].

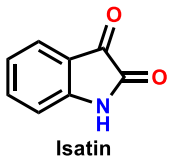

Isatin

Figure 8: Chemical structure of isatin

1.1.2. Isatin derivatives as anticancer agents

Researchers from academia and pharmaceutical companies have thoroughly investigated the anti-cancer properties of isatin and its derivatives in an effort to create isatin-based anticancer drugs [38,46,47]. These fantastic efforts resulted in the development of novel anticancer drugs including sunitinib, toceranib, and nintedanib that have received clinical approval. Semaxanib (SU5416) and orantinib (SU6668) are two other drugs with isatin scaffolds that demonstrated remarkable anti-cancer activity in clinical trials [48,49] (**Figure 9**). Analogs of isatin were discovered to be efficient against

several malignancies, including AML [50–52]. Moreover, the isatin-based drug sunitinib was approved for treatment gastrointestinal stromal tumor (GIST) and renal cell carcinoma (RCC) [53,54].

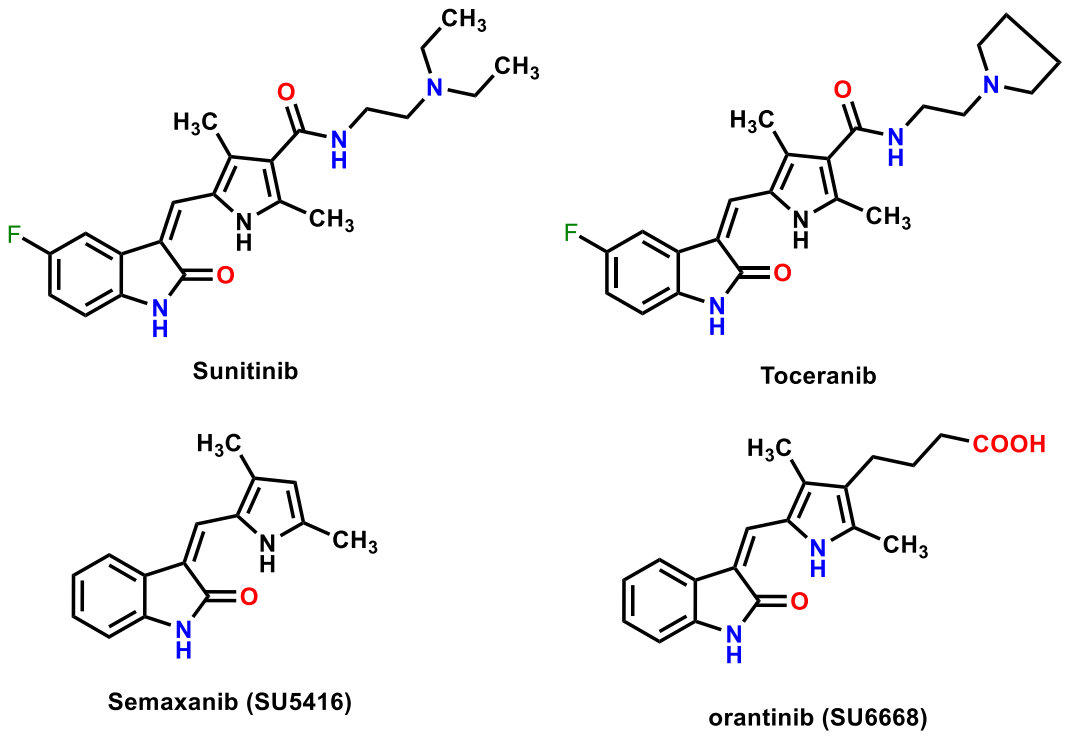

Figure 9: Chemical structures of isatin-based anticancer drugs

Isatin derivatives influence the expression of genes associated with apoptosis as well as a variety of biological targets, including histone deacetylases, carbonic anhydrases, tyrosine kinases, tubulin polymerization, and ERK1/2 phosphorylation [38,55–58].

1.1.3. α,β-Unsaturated carbonyl compounds as antineoplastic agents

The literature is well recognized for the anticancer properties of compounds containing the α,β-unsaturated ketone moiety, and these compounds are regarded as one of the most significant chemical structures in drug discovery [59,60]. They are extensively distributed in biologically active substances that have been effective in cancer therapy such as xanthohumol and the chemopreventive agent curcumin [61], (**Figure 10**). Because of the conjugated double bond, the α,β-unsaturated carbonyl moiety undergoes a

Michael addition type reaction with cellular thiols, thus these compounds are known as thiol alkylators [62]. However, this type of compounds shows very limited or no reactivity towards amino and hydroxyl groups which are found in nucleic acids [63] and thus are likely to be free from the carcinogenic and mutagenic properties of certain anticancer drugs. In comparison to normal tissues, it is discovered that the expression of cellular thiols is increased in a several malignancies [64,65]. As a result, it is sought that the anticancer activities of α,β-unsaturated carbonyl compounds are believed to be due to the ability to react with cellular thiols that play important roles in tumor progression and drug resistance [62]. A number of reviews have been written on α,β-unsaturated carbonyl compounds that provide further evidence of the potential usefulness of this type of compounds in cancer chemotherapy [59,60,66]. Besides the ability to interact with cellular thiols, α,β-unsaturated carbonyl compounds can induce apoptosis which is considered to be a major channel of physiological cell death and a promising therapeutic target for cancer treatment [61].

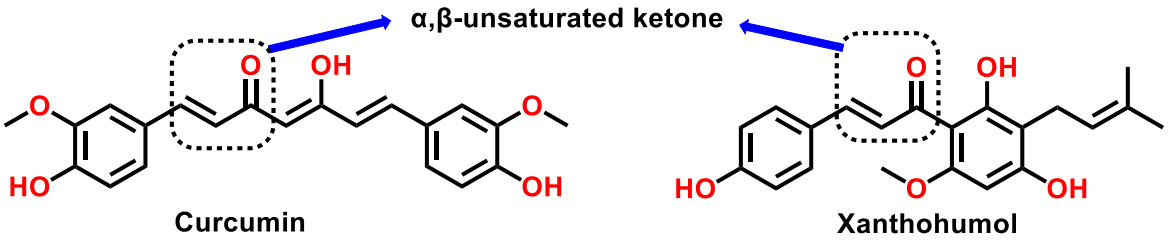

Figure10: Structures of natural products containing α,β-unsaturated ketone

1.2. Rational and design

According to a report, the oxindole scaffold, which can occupy the hinge area of the ATP binding domain in numerous kinases, is essential for the anticancer action of isatin derivatives [67]. Additionally, the hydrophobic tail of sunitinib, such as *N*,*N*-diethyl, is what binds to the allosteric site of different kinases [68]. As a result, in this study, the hydrophobic tail and the oxindole scaffold were kept together and connected by α,β-unsaturated ketone spacer.

We experimented with a variety of bio-isosteric changes in the hydrophobic tail, including piperidine **5c** or morpholine **5d** to rigidify the structure and extend the flexible *N*,*N*-diethyl moiety of sunitinib to *N*,*N*-dipropyl **5b**. Further investigation was done into extension to *N*-alkyl piperazine **5e**, *N*-acyl piperazine **5f** and **5g**, or *N*-heteroaryl piperazine **5h**.

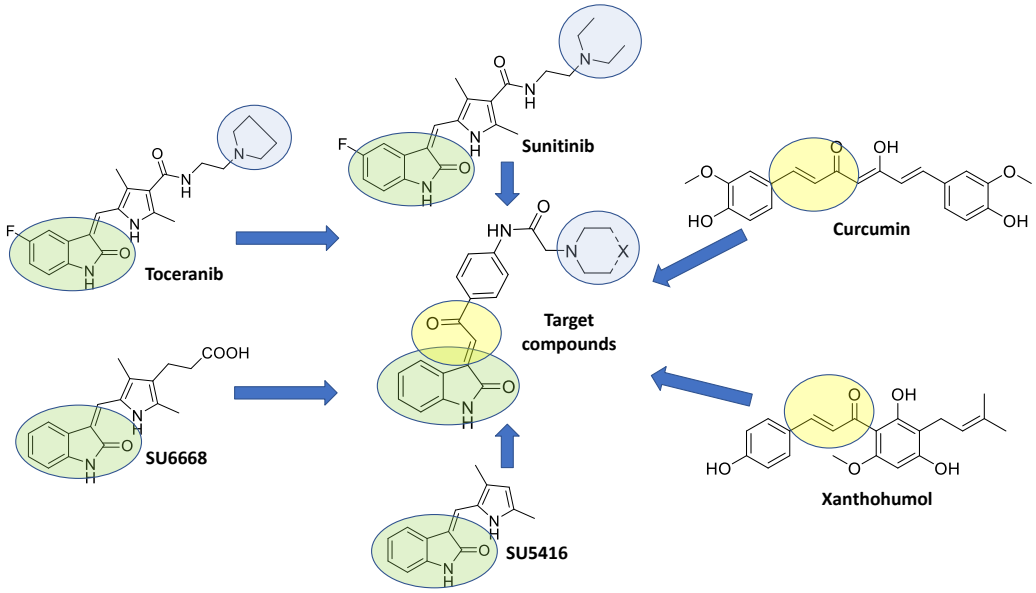

Figure 11: Rational design of the target compounds based on oxindole hybridization

1.3. Results and discussion

We proposed that combining these bioactive structural features in a single molecule may lead to the development of promising new lead compounds with potential anticancer activity. Our inspiration for this idea came from the structural characteristics of isatin-derived approved anticancer drugs and, α,β-unsaturated ketone.

1.3.1. Synthesis of isatin derivatives

As, outlined in **scheme 1**, the target compounds were through aldol condensation of ketonic carbonyl group in isatin **1** with the reactive α-methyl group in *p*-aminoacetophenone **2** in dehydrated ethanol in presence of diethylamine. The obtained white precipitate **3a** was collected by vacuum filtration washed with water and ethanol. Compound **3a** was dehydrated

through refluxing with hydrochloric acid in super dehydrated ethanol to afford the α,β-unsaturated ketone intermediate **3b**. Subsequently, the free amino group in compound **3b** was treated with chloroacetyl chloride in super dehydrated THF in presence of diisopropylethylamine (DIPEA) at 0 °C to provide 2-chloroacetmaide intermediate **4**. The final target compounds **5a-h** were obtained by nucleophilic substitution of 2-chloro in compound **4** with different aliphatic acyclic or cyclic secondary amines. All target compounds were obtained in good yields after purification using column chromatography and their structures were assured via NMR and mass spectroscopy.

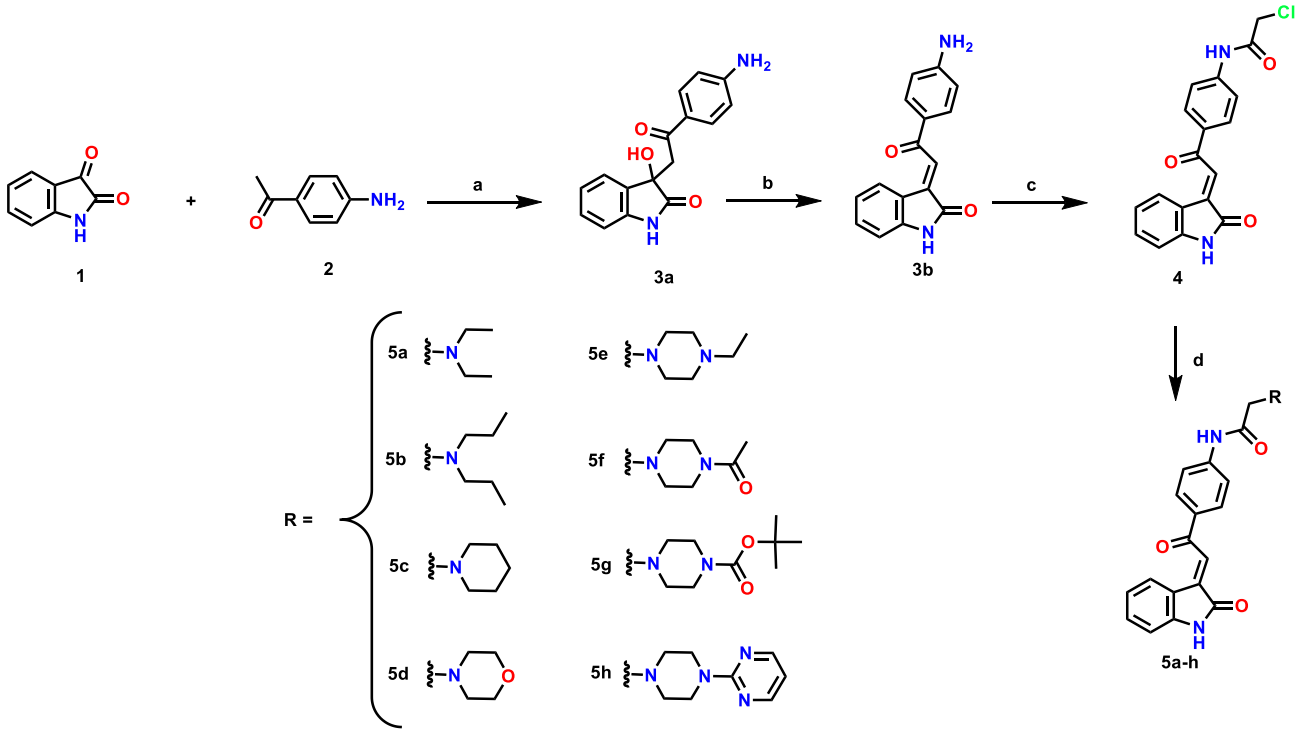

Scheme 1. Synthesis of the target compounds **5a-h**. Reagent and conditions: (a) EtOH, diethylamine, r.t., overnight; (b) EtOH, hydrochloric acid, reflux, 3 h; (c) Chloroacetyl chloride, DIPEA, THF, 0 ^{0}C, 20 min. then r.t., 3 h; (d) Secondary amine, potassium iodide, DMF, r.t., 3 h.

1.3.2. Biological evaluation

1.3.2.1. Evaluation of the *in vitro* cytotoxic activity

To evaluate the impact of synthesis of novel isatin hybrids including α, β-unsaturated ketone **5a-h** on their cytotoxic activity against several cancer cell lines derived from different body organs and tissues, all compounds were

submitted to National Cancer Institute (NCI), Bethesda, within the Developmental Therapeutics Program (DTP). All compounds were selected by NCI for *in vitro* screening of anticancer activity according to the protocol of the Drug Evaluation Branch of the National Cancer Institute [69].

By using a main *in vitro* one-dose experiment at a single concentration (10 μM), the cytotoxic activity was assessed against 60 cell lines originating from nine tumor subpanels, including cell lines from leukemia, melanoma, the lung, colon, CNS, ovarian, renal, prostate, and breast cancers. **Figures 12–19** show the percentage of cells in each cell line that grew *in vitro*. By deducting the growth percentage from 100, the *in vitro* growth inhibition percentage (GI%) was obtained (GI% = 100 - growth percentage). Lethality is shown by growth percentages with negative values; for example, growth percentage of -40 would represent 40% lethality. GI%, mean GI% and lethality% were calculated and outlined in **table 1** and **Figure 20**.

The synthesized compounds have substantial cytotoxic activity against several cancer cell lines, according to results of NCI-60 screening. All compounds showed outstanding activity against leukemia cell lines especially acute myeloid leukemia (AML) cells HL-60 and acute lymphoblastic leukemia (ALL) cells MOLT-4. Compounds **5b** and **5g**, for instance, demonstrated 43.91% and 46.44% lethality against HL-60 and 31.26% and 44.85% lethality against Molt-4 cells, respectively. The human colorectal cancer cell lines HCT116 and SW-620, in particular, showed the greatest sensitivity to all synthesized compounds, demonstrating their potent anti-colorectal effects.

For instance, treatment of HCT116 and SW-620 cells with compound **5b** resulted in lethality percentages of 88.15% and 76.08%, respectively, and in the same way, compound **5g** exerted strong lethality on HCT116 and SW-620 cells (96.98% and 88.72%, respectively). When it came to cells originated from non-small cell lung cancer, HOP-92, NCI-H226 and NCI-H22 were the most

affected cell lines while the tested compounds showed weak growth inhibition against A549/ATCC with GI% values ranging from 5.75% to 25.07%. Glioblastoma cell line SF-539 was the most affected among CNS cancer cell lines, and **5a** showed a 58.59% growth inhibition. Moreover, **5b** and **5g** induced lethality of 35.29% and 72.33% in SF-539, respectively.

Additionally, the synthesized compounds manifested amazing activity against various melanoma cancer cell lines, especially LOX IMVI cells. Where, compound **5h** inhibit cells growth by 59.67%, while compounds **5a**, **5b** and **5g** induced lethality of LOX IMVI cells by 61.45%, 98.98 and 100%, respectively.

The synthesized compounds exhibited good to excellent activities against all renal cancer cell lines except A498. Likewise, the compounds affected growth of prostate cancer cell line P53 with GI% between 4.42% and 74.73%. Finally, amazing cytotoxic activity against breast cancer cell lines, particularly MCF-7, was demonstrated by all synthesized compounds. Additionally, the compounds had exceptional cytotoxicity against the MDA-MB-486 triple negative breast cancer cell line, with GI% ranging from 49.41% to 76.47%, while **5g** caused 67.01% lethality.

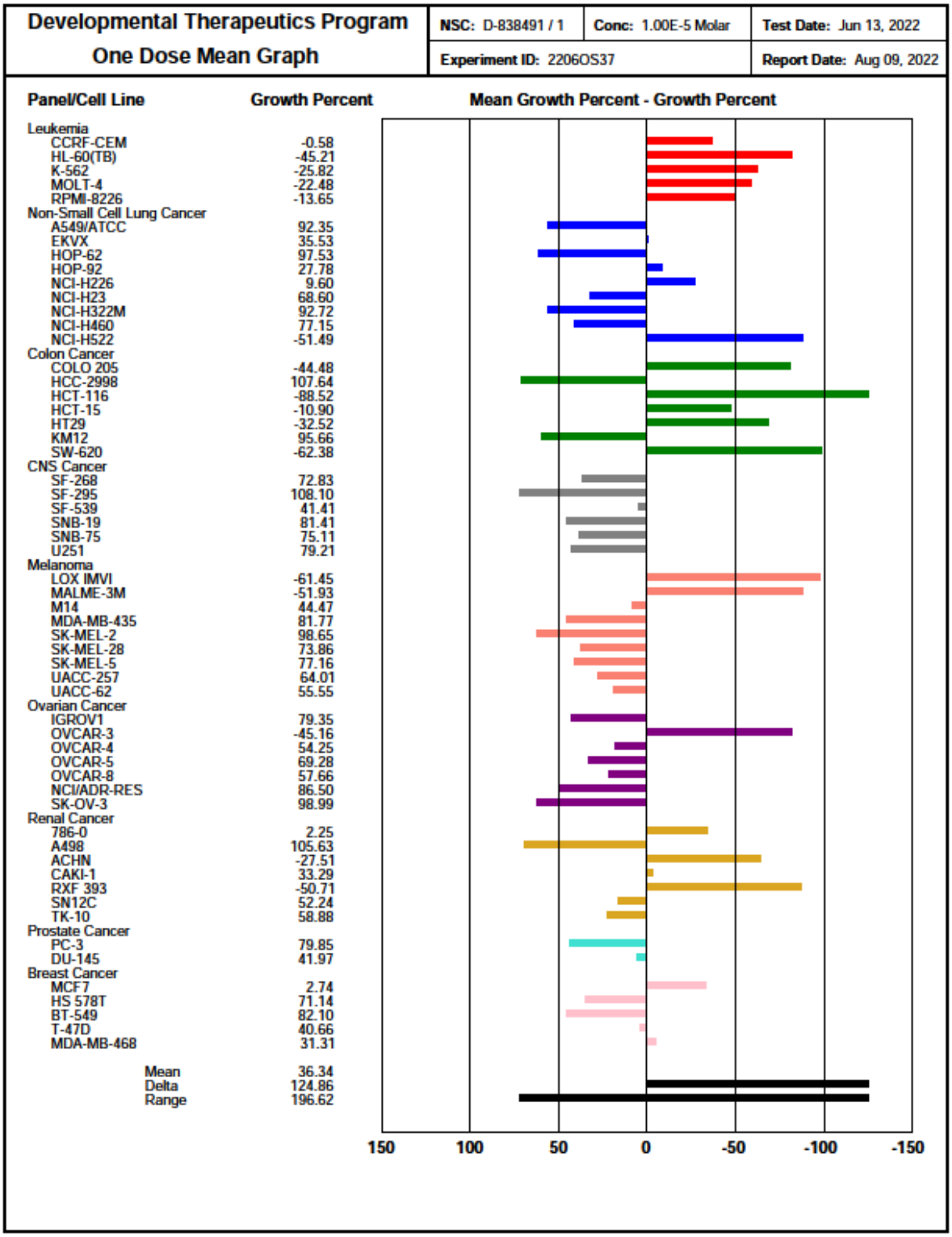

Figure 12: One-dose mean graph of compound **5a** against different cancer cell lines based on SRB assay at NCI at 10 µM concentration after 48 h.

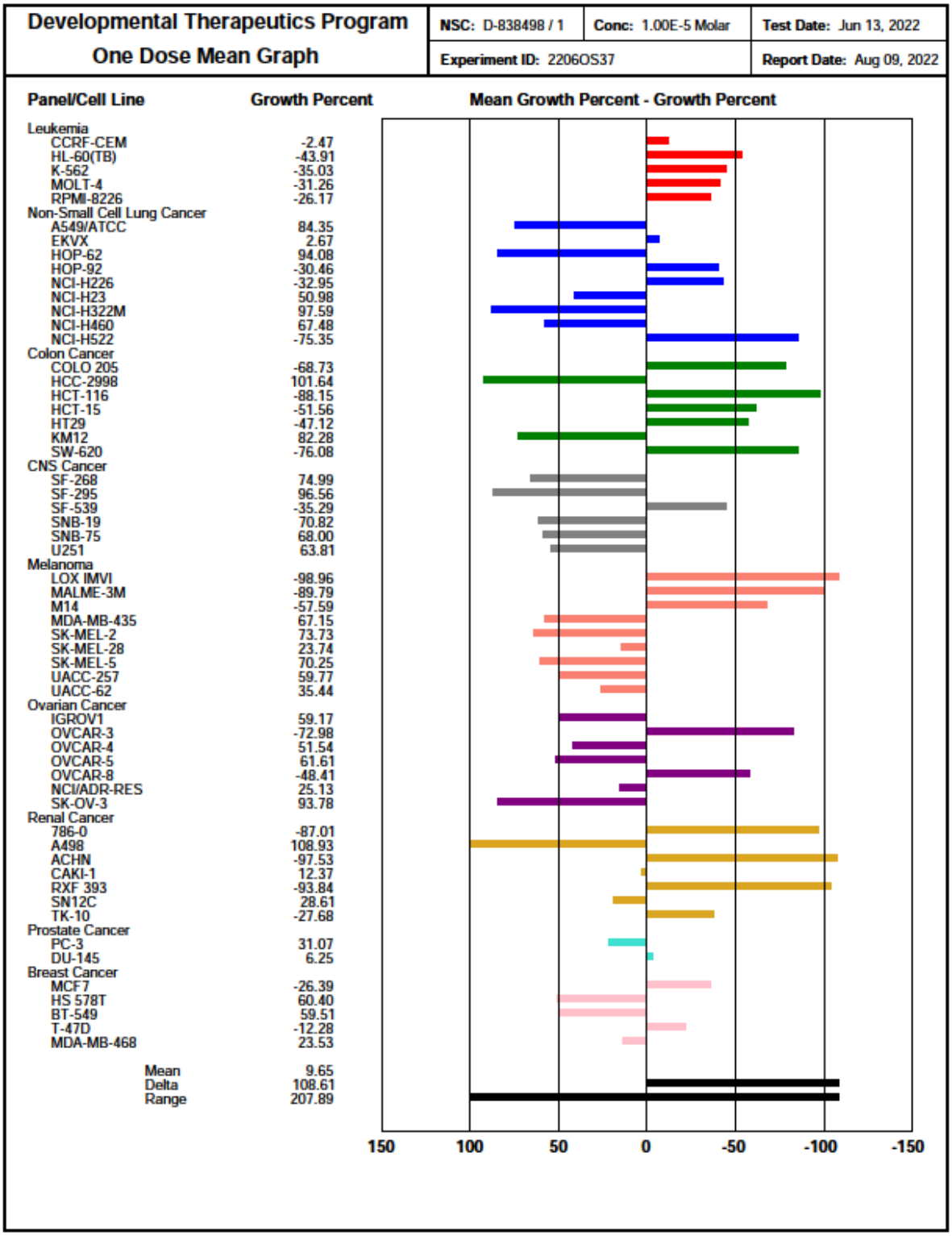

Figure 13: One-dose mean graph of compound **5b** against different cancer cell lines based on SRB assay at NCI at 10 µM concentration after 48 h.

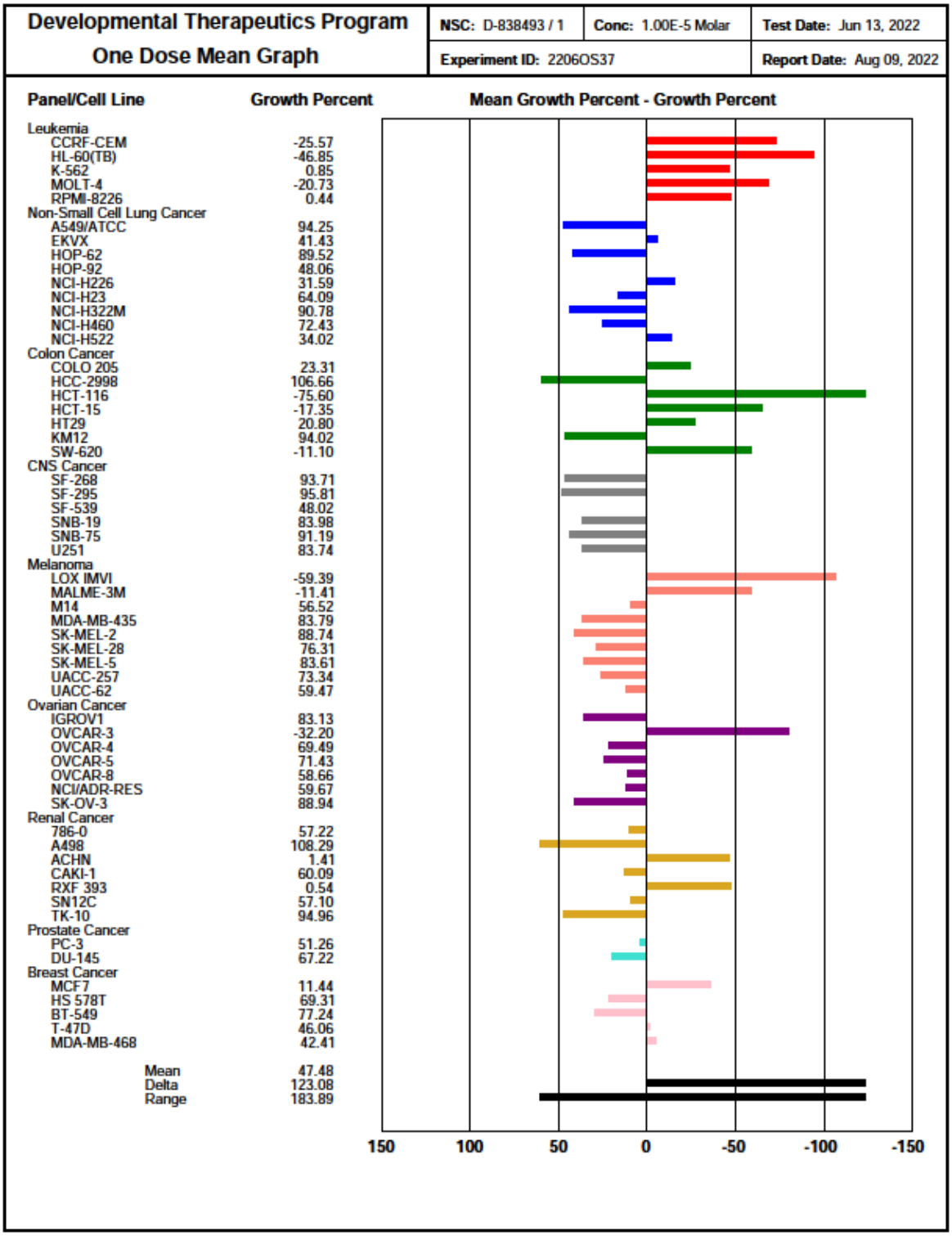

Figure 14: One-dose mean graph of compound **5c** against different cancer cell lines based on SRB assay at NCI at 10 µM concentration after 48 h.

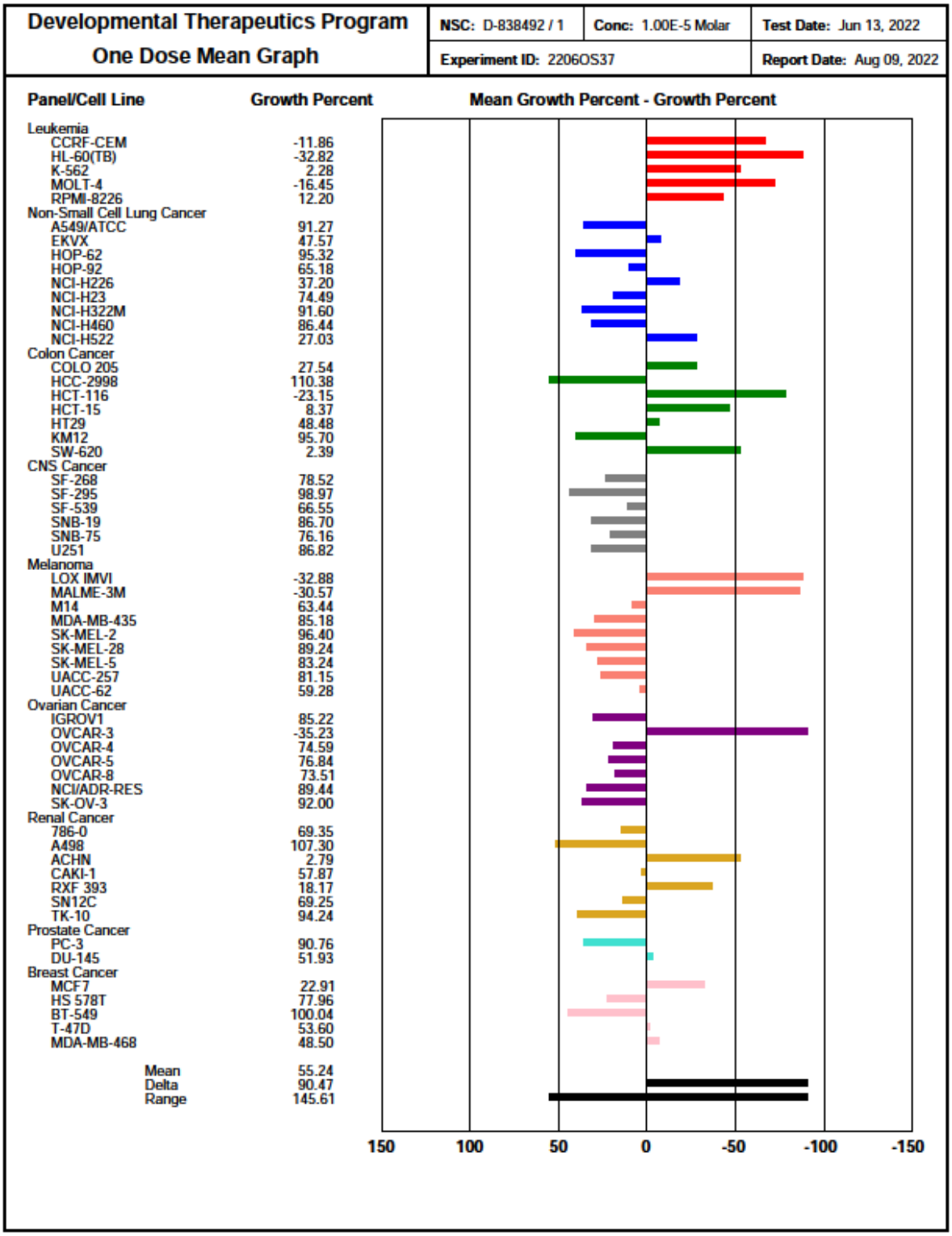

Figure 15: One-dose mean graph of compound **5d** against different cancer cell lines based on SRB assay at NCI at 10 µM concentration after 48 h.

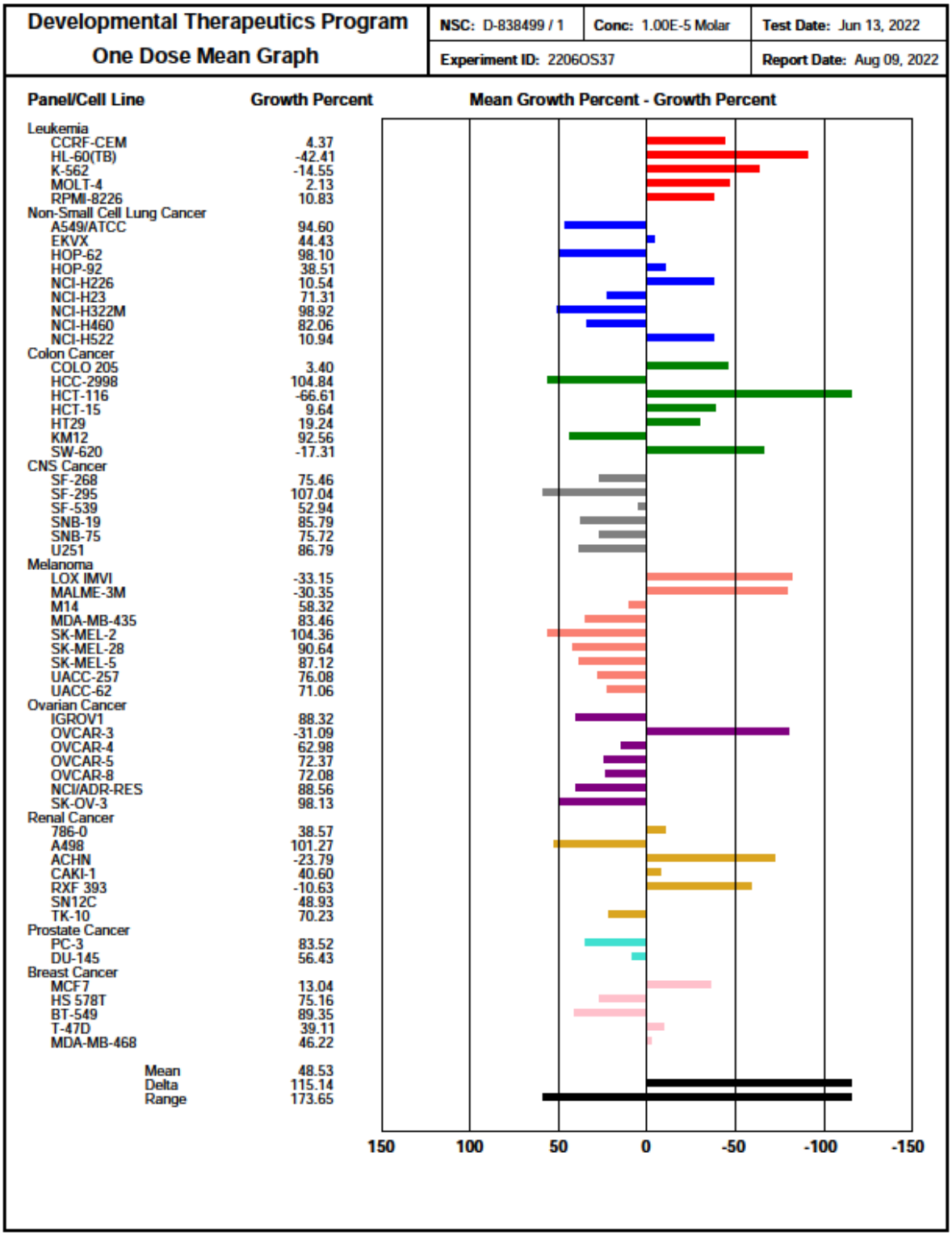

Figure 16: One-dose mean graph of compound **5e** against different cancer cell lines based on SRB assay at NCI at 10 µM concentration after 48 h.

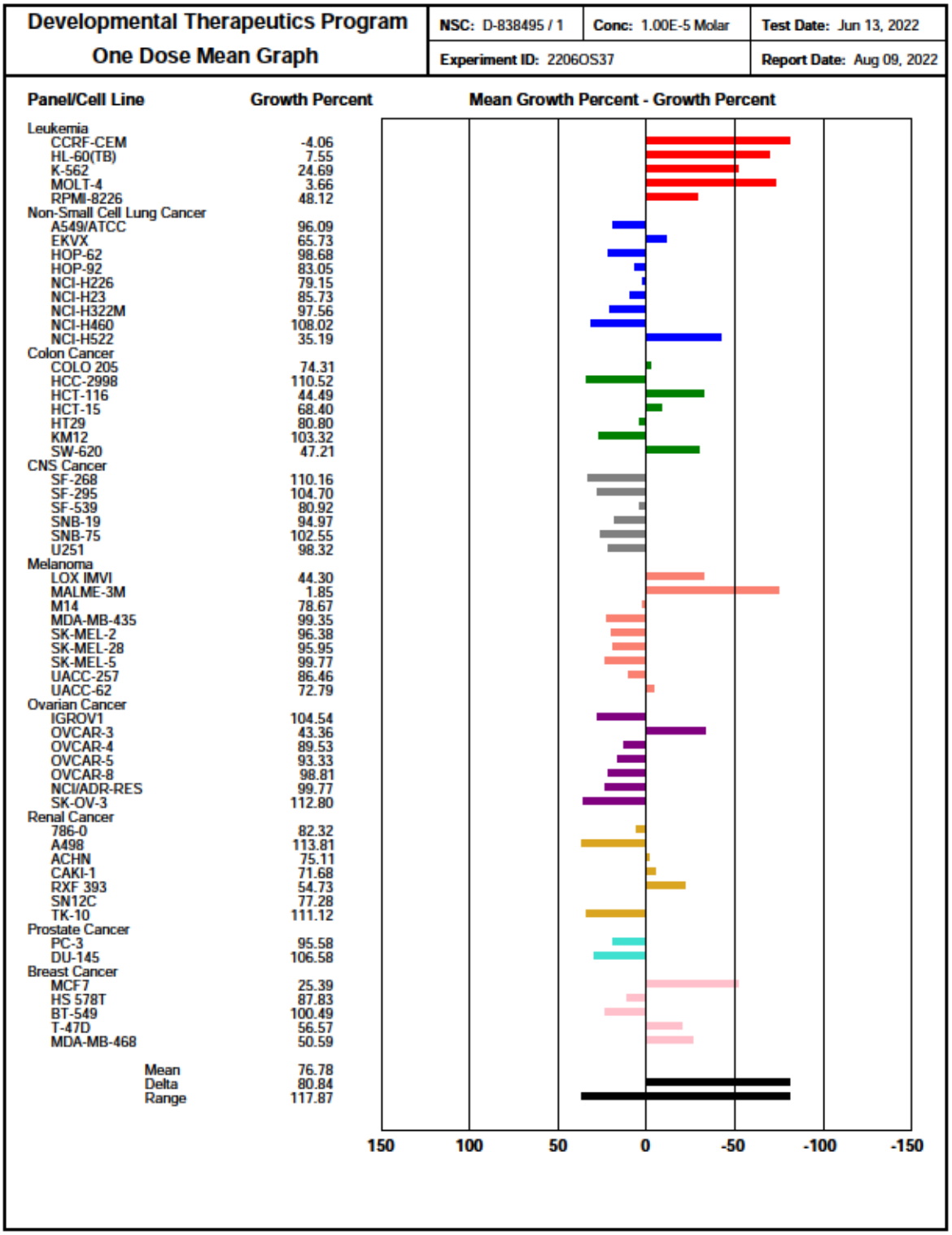

Figure 17: One-dose mean graph of compound **5f** against different cancer cell lines based on SRB assay at NCI at 10 µM concentration after 48 h.

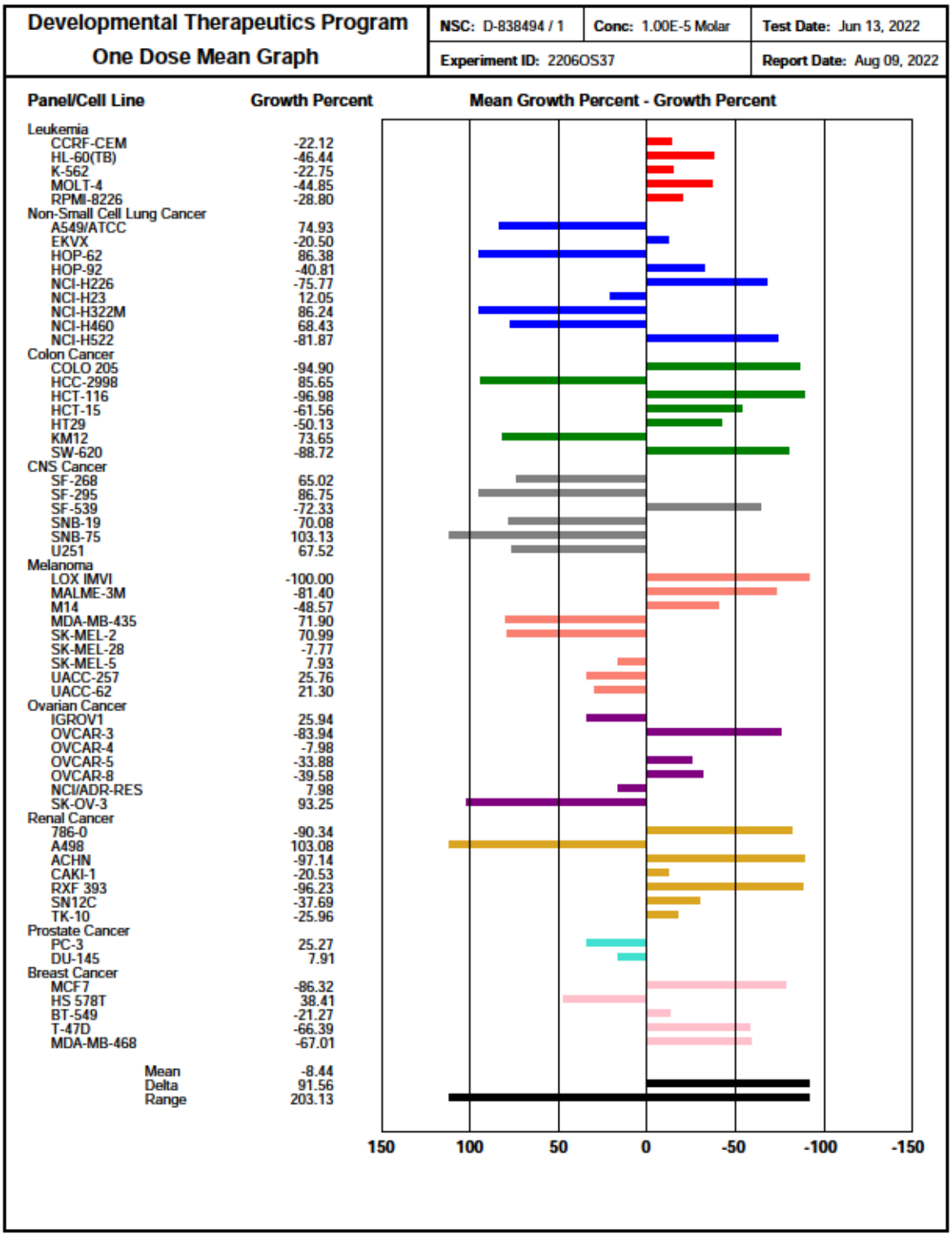

Figure 18: One-dose mean graph of compound **5g** against different cancer cell lines based on SRB assay at NCI at 10 µM concentration after 48 h.

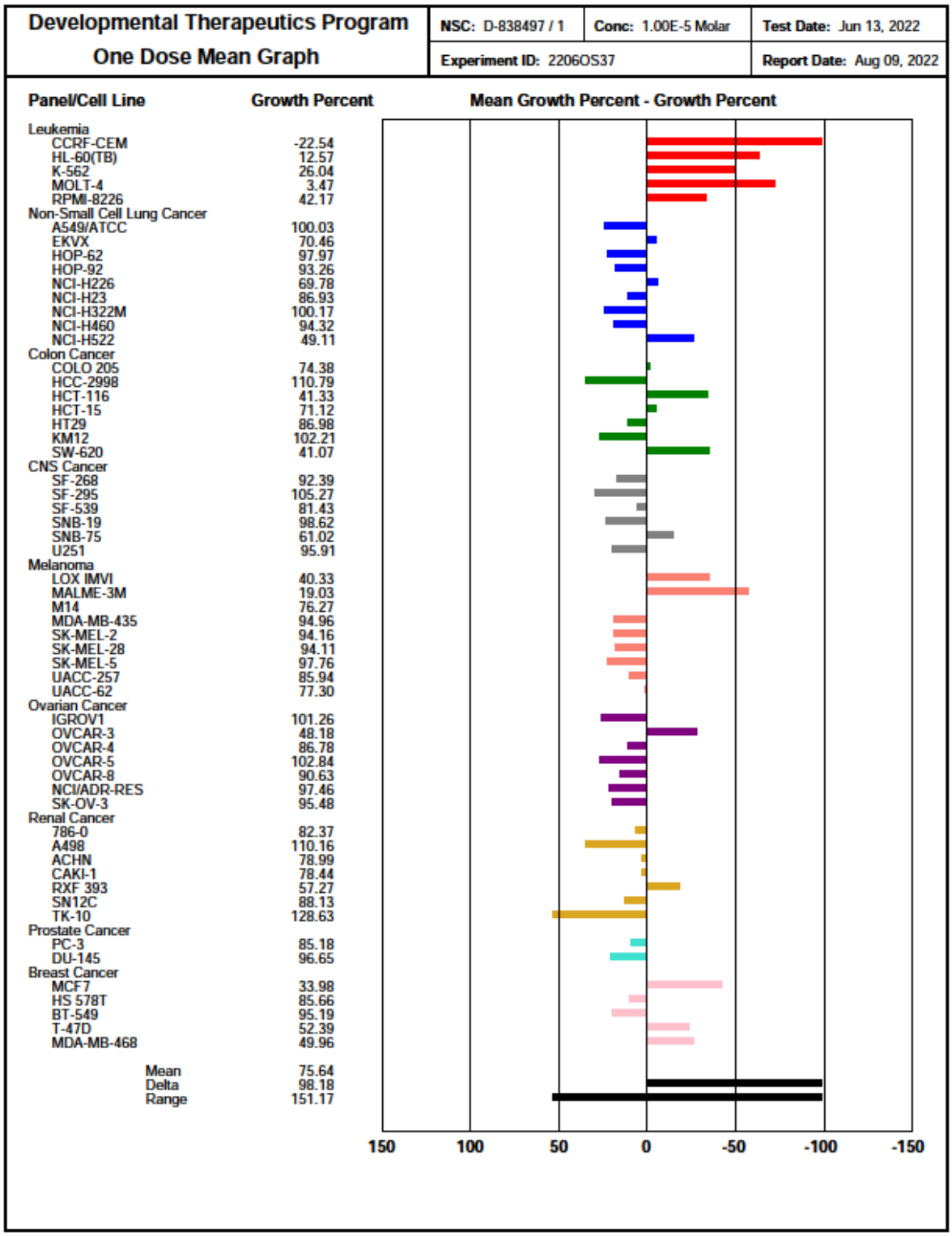

Figure 19: One-dose mean graph of compound **5h** against different cancer cell lines based on SRB assay at NCI at 10 µM concentration after 48 h.

Table 1. *In vitro* growth inhibition and lethality obtained from the single dose (10μM) test of compounds **5a-h**

Panel	Cell line	Growth inhibition (GI) percent at 10 μM							
		5a	**5b**	**5c**	**5d**	**5e**	**5f**	**5g**	**5h**
Leukemia	CCRF-CEM	-0.58	-2.47	-25.57	-11.86	95.63	-4.06	-22.12	-22.54
	HL-60(TB)	-45.21	-43.91	-46.85	-32.82	-42.41	92.45	-46.44	87.43
	K-562	-25.82	-35.03	99.15	97.72	-14.55	75.31	-22.75	73.96
	MOLT-4	-22.48	-31.26	-20.73	-16.45	97.87	96.34	-44.85	96.53
	RPMI-8226	-13.65	-26.17	99.56	87.8	89.17	51.88	-28.80	57.83
Non-Small Cell Lung Cancer	A549/ATCC	7.65	15.65	5.75	8.73	5.40	3.91	25.07	-
	EKVX	64.47	97.33	58.57	52.43	55.57	34.27	-20.50	29.54
	HOP-62	2.47	5.92	10.48	4.68	1.90	1.32	13.62	2.03
	HOP-92	72.22	-30.46	51.94	34.82	61.49	16.95	-40.81	6.74
	NCI-H226	90.40	-32.95	68.41	62.8	89.46	20.85	-75.77	30.22
	NCI-H23	31.40	49.02	35.91	25.51	28.69	14.27	87.95	13.07
	NCI-H322M	7.28	2.41	9.22	8.40	1.08	2.44	13.76	-
	NCI-H460	22.85	32.52	27.57	13.56	17.94	-	31.57	5.68
	NCI-H522	-51.49	-75.35	65.98	72.97	89.06	64.81	-81.87	50.89
Colon Cancer	COLO 205	-44.48	-68.73	76.69	72.46	96.60	25.69	-94.90	25.62
	HCC-2998	-	-	-	-	-	-	14.35	-
	HCT-116	-88.52	-88.15	-75.60	-23.15	-66.61	55.51	-96.98	58.67
	HCT-15	-10.90	-51.56	-17.35	91.63	90.36	31.60	-61.56	28.88
	HT29	-32.52	-47.12	79.2	51.52	80.76	19.20	-50.13	13.02
	KM12	4.34	17.72	5.98	4.3	7.44	-	26.35	-
	SW-620	-62.38	-76.08	-11.10	97.61	-17.31	52.79	-88.72	58.93
CNS Cancer	SF-268	27.17	25.01	6.29	21.48	24.54	-	34.98	7.61
	SF-295	-	3.44	4.19	1.03	-	-	13.25	-
	SF-539	58.59	-35.29	51.98	33.45	47.06	19.08	-72.33	18.57
	SNB-19	18.59	29.18	16.02	13.30	14.21	5.03	29.92	1.38
	SNB-75	24.89	32.00	8.81	23.84	24.28	-	-	38.98
	U251	20.79	36.19	16.26	13.18	13.21	1.68	32.48	4.09

Melanoma	LOX IMVI	-61.45	-98.96	-59.39	-32.88	-33.15	55.70	-100	59.67
	MALME-3M	-51.93	-89.79	-11.41	-30.57	-30.35	98.15	-81.40	80.97
	M14	55.53	-57.59	43.48	36.56	41.68	21.33	-48.57	23.73
	MDA-MB-435	18.23	32.15	16.21	14.82	16.54	0.65	28.10	5.04
	SK-MEL-2	1.35	26.27	11.26	3.60	-	3.62	29.01	5.84
	SK-MEL-28	26.14	76.26	23.69	10.76	9.36	4.05	-7.77	5.89
	SK-MEL-5	22.84	29.75	16.39	16.76	12.88	0.23	92.07	2.24
	UACC-257	35.99	40.23	26.66	18.85	23.92	13.54	74.24	14.06
	UACC-62	44.45	64.56	40.53	40.72	28.94	27.21	78.70	22.70
Ovarian cancer	IGROV1	20.65	40.83	16.87	14.78	11.68	-	74.06	-
	OVCAR-3	-45.16	-72.98	-32.20	-35.23	-31.09	56.64	-83.94	51.82
	OVCAR-4	45.75	48.46	30.51	25.41	37.02	10.47	-7.98	13.22
	OVCAR-5	30.72	38.39	28.57	23.16	27.63	6.67	-33.88	-
	OVCAR-8	42.34	-48.41	41.34	26.49	27.92	1.19	-39.58	9.37
	NCI/ADR-RES	13.50	74.59	40.33	10.56	11.44	0.23	92.02	2.54
	SK-OV-3	1.01	6.23	11.06	8.00	1.87	-	6.75	4.52
Renal Cancer	786-0	97.75	-87.01	42.78	30.65	61.43	17.68	-90.34	17.63
	A498	-	-	-	-	-	-	-	-
	ACHN	-27.51	-97.53	98.59	97.21	-23.79	24.89	-97.14	21.01
	CAKI-1	66.71	87.63	39.91	42.13	59.4	28.32	-20.53	21.56
	RXF 393	-50.71	-93.84	99.46	81.83	-10.63	45.27	-96.23	42.73
	SN12C	47.76	71.39	42.9	30.75	51.07	22.72	-37.69	11.87
	TK-10	41.12	-27.68	5.04	5.76	29.77	-	-25.96	-
Prostate Cancer	PC-3	20.15	68.93	48.74	9.24	16.48	4.42	74.73	14.82
	DU-145	68.03	93.75	32.78	48.07	43.57	-	92.09	3.35
Breast Cancer	MCF7	97.26	-26.39	88.56	77.09	86.96	74.61	-86.32	66.02
	HS 578T	28.86	39.6	30.69	22.04	24.84	12.17	61.59	14.34
	BT-549	17.90	40.49	22.76	-	10.65	-	-21.27	4.81
	T-47D	59.34	-12.28	53.94	46.40	60.89	43.43	-66.39	47.61
	MDA-MB-468	68.69	76.47	57.59	51.50	53.78	49.41	-67.01	50.04
Mean		63.66	90.35	52.52	44.76	51.47	23.22	-8.44	24.36

We can draw the conclusion that the current hybrid strategy is a successful method for obtaining novel compounds with remarkable antiproliferative activity against various cancer types based on the NCI screening data. The antiproliferative activity was greatly improved when the *N*,*N*-diethyl **5a** (mean GI=63.66) acyclic hydrophobic tail was extended to the longer *N*,*N*-dipropyl **5b**, where the mean GI% increased to 90.45. On the contrary, substituent rigidification by using piperidine **5c** or morpholine **5d**, instead of *N*,*N*-diethyl **5a**, led to a trivial drop of the activity with mean GI% values of 52.52 and 44.76, respectively.

In a similar vein, substitution with *N*-ethyl piperazine **5e** afforded slightly less potent compounds like **5c** and **5d**. While substitution of ethyl group in *N*-ethylpiperazine **5e** with acetyl group **5f** resulted in a dramatic activity decline with mean GI% of 23.22, but extension of the group attached to piperazine nitrogen to *t*-butyloxycarbonyl **5g** instead of acetyl group **5f** highly escalated the activity with a mean value of 8.44% lethality. When the *t*-butyloxycarbonyl group **5g** was replaced with the planar pyrimidine ring **5h**, the activity decreased again to a similar value of **5f**. In a word, compounds **5b** and **5g** are the most active compounds within the series.

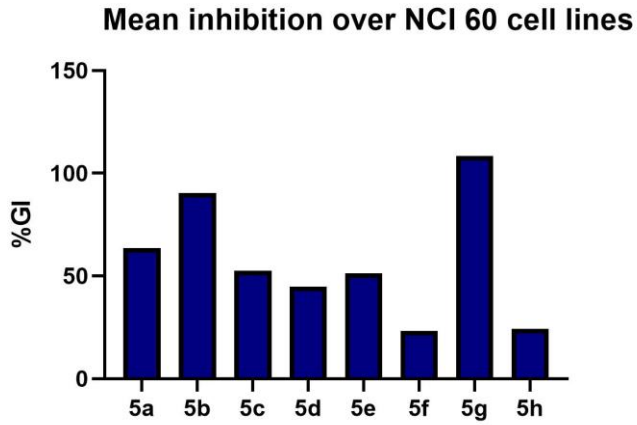

Figure 20: Graphical representation of the mean inhibition percentages calculated according to GI% values over NCI-60 cell lines.

Motivated by these intriguing NCI cytotoxicity results, we attempted to determine the IC_{50} values of synthesized compounds against proliferation of acute myeloid leukemia HL-60 cells, as it was one of the most sensitive cell lines in the one dose screening. In this experiment, the highly potent kinase inhibitor staurosporine was used as reference. Upon treatment of cells with different doses from the synthesized compounds, it revealed impressive cytotoxicity with sub-micromolar IC_{50} values for compounds **5a**, **5b**, **5g** and **5h**, as shown in **Table 2**. Compounds **5b** and **5g** were the most potent with IC_{50} values 0.38 ± 0.08 µM and 0.57 ± 0.05 µM which are comparable with the positive control staurosporine. In order to assess the safety of the synthesized compounds, we screened the cytotoxicity of the most potent compound **5b** on the normal peripheral blood mononuclear cells PBMC. The compound showed weak cytotoxicity on normal cells with IC_{50} value 14.17 µM, and selectivity index (SI) 37.2. these results explore that the synthesized compounds have selective cytotoxic activity against cancer cells without affecting body normal cells. Therefore, the target compounds are promising anticancer lead compounds.

Table 2: *In vitro* cytotoxicity IC_{50} (µM) results against acute myeloid leukemia cells HL-60 and normal peripheral blood mononuclear cells PBMC and selectivity index (SI) which was calculated as the ratio of cytotoxicity (IC_{50}) of normal cells (PBMC) to cancer cells (HL-60).

Cells	5a	5b	5c	5d	5e	5f	5g	5h	Staurosporine
HL-60	0.72 ± 0.09	0.38 ± 0.08	1.06 ± 0.10	1.43 ± 0.16	1.07 ± 0.13	2.57 ± 0.29	0.57 ± 0.05	0.79 ± 0.08	0.013 ± 0.002
PBMC	-	14.17± 1.13	-	-	-	-	-	-	-
SI	-	37.2	-	-	-	-	-	-	-

All IC_{50} values are the mean ± standard error of three different experiments.

- : not tested.

1.3.2.2. Analysis and discrimination of apoptosis and necrosis

Apoptosis is a natural mechanism for programed cell death [70]. It plays a critical role in development as well as homeostasis [71]. It is tightly controlled process that is necessary for elimination of any extra or undesirable cells The

activation of the apoptotic pathway can be caused by a wide range of circumstances, such as DNA damage or uncontrolled proliferation [72]. As soon as apoptosis is signaled, changes start to occur within the cell. These changes include activation of caspases which cleave cellular components required for normal cellular function such cytoskeletal and nuclear proteins. Apoptotic cells start to contract and experience alterations to their plasma membranes as a result of caspase activation, which triggers the macrophage response [73].

To elucidate the effect of the synthesized compounds on apoptosis induction, Annexin V-FTIC/7-AAD dual staining assay was conducted for the most active compounds **5b** and **5g** on HL-60 cells. As outlined in **Figure 21**, upon treating HL-60 cells with compounds **5b** and **5g** for 12 h and 24 h, both compounds induced apoptosis by about two folds increase in early apoptosis in 12 h incubation time. Moreover, both compounds demonstrated two folds increase in the percentage of late apoptosis/necrosis at 24 h incubation time compared with the control. These findings supported the hypothesis that the target chemicals primarily influence cancer cells by inducing apoptosis.

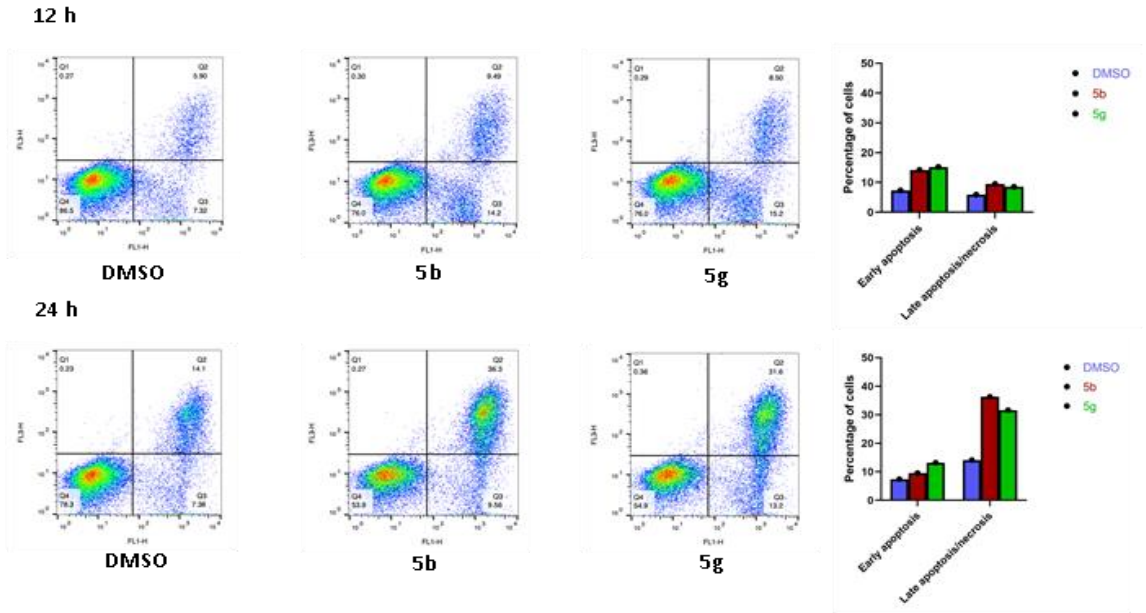

Figure 21: Apoptosis analysis of **5b** and **5g** using Annexin V-FITC/7-AAD dual staining in HL-60 cells.

1.3.2.3. Cell cycle analysis

Because of mutations that permit cell cycle progression and impede exit, cancer cells keep dividing. A significant consequence is that all cancers depend on continuous cell division, and many become increasingly dependent on remaining cell cycle control mechanisms to prevent the excessive accumulation and propagation of genome instability [74].

Using flow cytometric analysis on HL-60 cells, the impact of the two most active drugs, **5b** and **5g**, on cell cycle distribution was evaluated. Upon treatment of cells with compounds **5b** and **5g** for 24 hours, both compounds showed increase in percentage of cells in G1 phase compared with the control as depicted in **Table 3** and **Figure 22**. This data revealed that the target compounds can arrest cell cycle in the G1 phase.

Table 3. Effect of compound **5b** and **5g** on cell cycle distribution in HL-60 cells.

Sample	Cell Cycle Distribution (%)		
	%G0-G1	%S	%G2/M
DMSO / HL-60	61	16.7	21.5
5b/HL-60	68.8	10.3	20.1
5g/HL-60	67.5	15.6	16.7

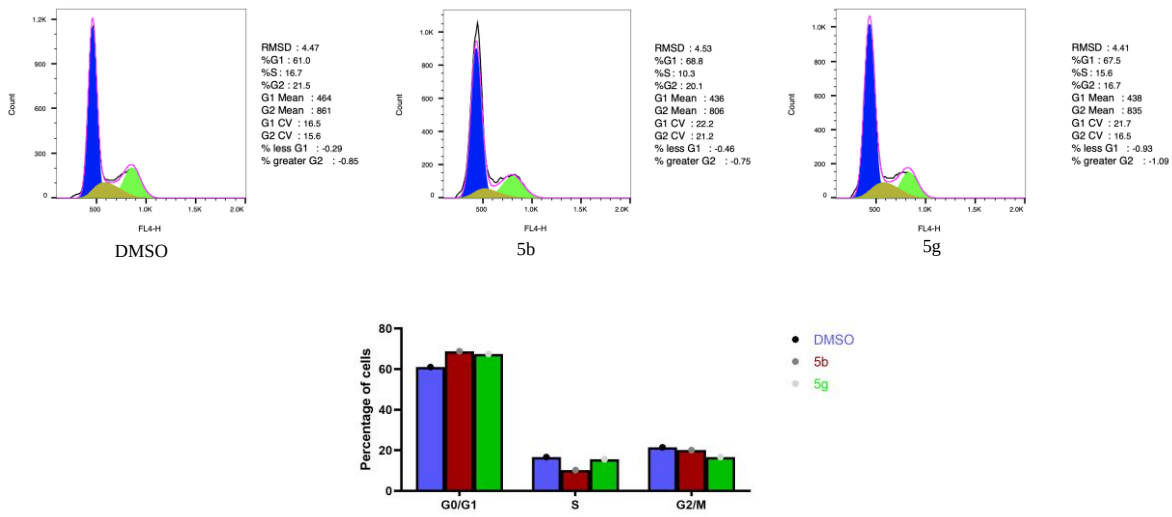

Figure 22: Cell cycle analysis of the HL-60 cells treated with compound **5b** and **5g** for 24 h using flow cytometry.

1.3.2.4. Western blot analysis

I used Swiss target prediction tool [75,76] in order to investigate the mechanism of action of the synthesized compounds and the most probable target inside the cells. Swiss target prediction tool showed that ERK1/2 are among the most probable targets of the synthesized compounds. I measured the effect of the most active compounds, **5b** and **5g**, on the phosphorylation of ERK1/2 in HL-60 cells based on the outcomes of molecular target prediction using the Swiss target prediction program. Where, HL-60 cells were incubated with compounds **5b** and **5g** for 24h, then level of phosphorylated ERK1/2 (p-ERK1/2) were evaluated using western blot analysis.

According to the findings, which are shown in **Figure 23**, the target compounds strongly inhibited ERK1/2 phosphorylation by around 60% and 80% for compounds **5b** and **5g**, respectively. The cytotoxic activity of compounds **5b** and **5g**, induction of apoptosis, and G1 phase cell cycle arrest appear to be attributed to their effect on ERK1/2 phosphorylation [11,77].

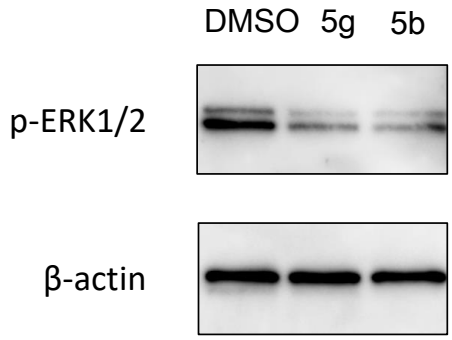

Figure 23: Effect of compound **5b** and **5g** on the immunoblotting of p-ERK1/2 proteins (normalized to β-actin).

1.3.3. *In silico* screening studies

1.3.3.1. Molecular docking

Most ERK inhibitors in clinical trials are ATP competitive, inhibiting ERK1/2 catalytic activity without impairing their phosphorylation by MEK or

nuclear translocation of p-ERK. The phosphorylation of ERK1/2 by MEK as well as its catalytic activity can both be inhibited by the specific, potent ERK1/2 inhibitor SCH772984 [11]. As a result, SCH772984 can entirely block MAPK pathway signaling and overcome emergence of resistance in MAPK pathway. Crystal structure of ERK2 co-crystallized with SCH772984 revealed that it binds to altered conformation of ERK2 in which Tyr36 in the glycine-rich loop (P-loop) becomes tucked under the loop as depicted in **Figure 24**. Binding of SCH772984 is hypothesized to be responsible for its ability to block ERK1/2 phosphorylation.

The synthesized compounds were virtually screened within the binding site of SCH772984 with ERK2 in order to validate the observed action of **5b** and **5g** on levels of ERK phosphorylation. From the protein data bank, the crystal structure of ERK2 co-crystallized with SCH772984 (PDB ID: 6GDM) was downloaded[11,78]. Using the commercial program Molecular Operating Environment (MOE 2019), the most active compounds (**5b** & **5g**) were docked into the reported binding site of SCH772984 with redocking the native ligand (SCH772984) for validation of the obtained results.

Docking results analysis of the 2D and 3D poses, **Figure 24**, illustrated that they were well-fitted on the ERK2 binding site and exhibited optimistic interactions with the key amino acid residues. The most active compounds **5b** and **5g** showed binding to the key amino acids inside the ATP hinge and the glycine rich loop (P-loop). Compound **5b** interacted at the hinge region through hydrogen binding with Lys114, also it showed hydrogen binding with Lys54 and pi-pi interaction with Tyr36 at the p-loop. In contrast, compound **5g** revealed hydrogen binding with Met108 at the hinge and Lys54 at the p-loop. Therefore, compounds **5b** and **5g** illustrated the same binding theme as SCH772984 and their binding energies scores (-8.8002 Kcal/mol and -8.6110 Kcal/mol respectively) are comparable with that of SCH772984 (-9.8950

Kcal/mol). The docking study results, and the western blot results support the hypothesis that the synthesized compounds bind to ERK and block its phosphorylation.

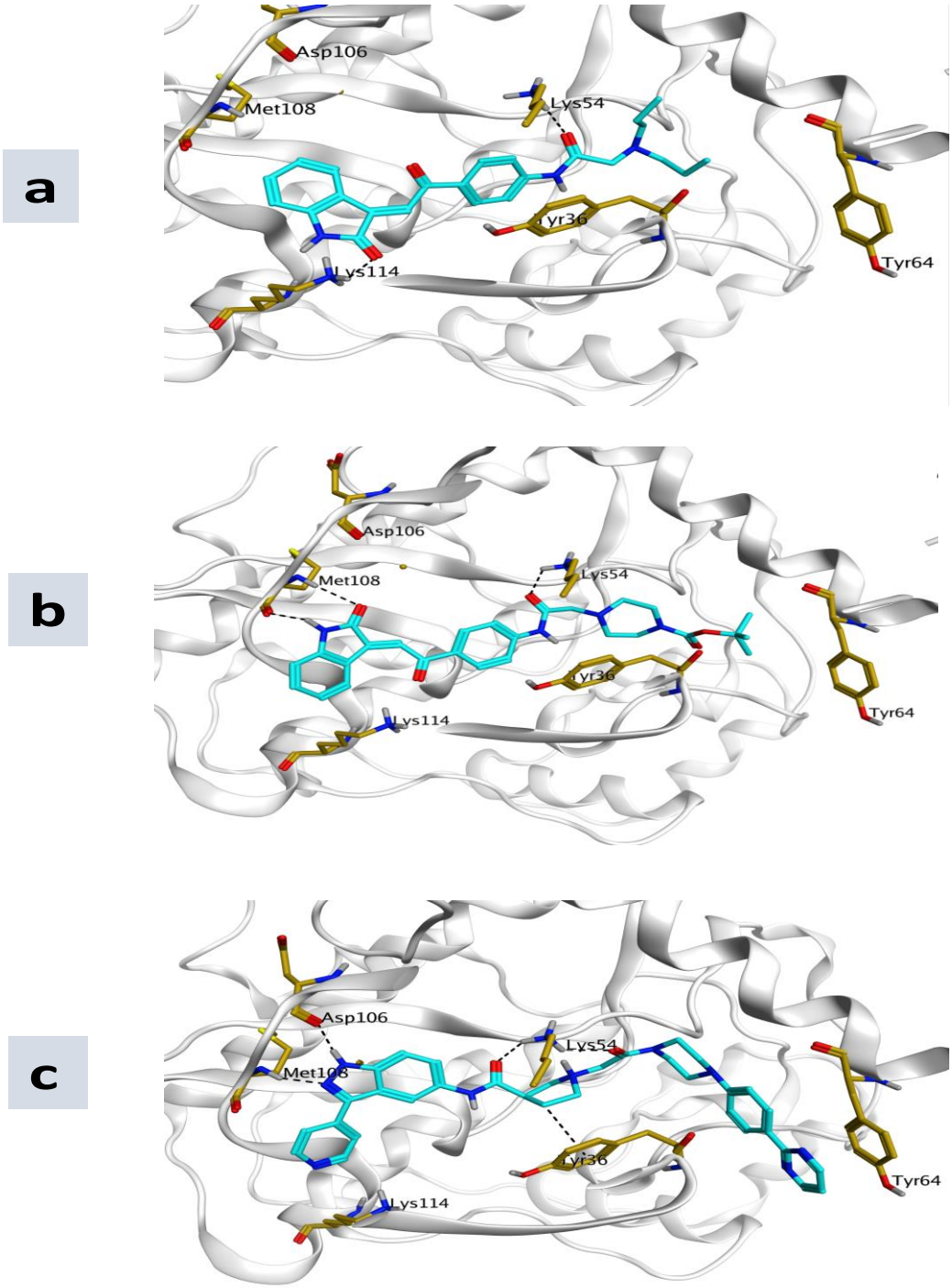

Figure 24: (**a**) 3D representation of the docking of **5b** in the active site of ERK2 (PDB ID: 6GDM); (**b**) 3D representation of the docking of **5g** in the active site of ERK2 (PDB ID: 6GDM); and (**c**) 3D representation of the docking of SCH772984 in the active site of ERK2 (PDB ID: 6GDM).

1.3.3.2. *In silico* prediction of physicochemical and pharmacokinetic properties

In the field of medicinal chemistry and drug discovery, appropriate pharmacokinetics properties are very significant as efficacy and safety. Due to their improper pharmacokinetics, many potent compounds fail to be drugs. In the current study, SwissADME website (http://www.swissadme.ch/index.php) was utilized for prediction of the physicochemical and pharmacokinetic properties of the synthesized compounds (**5a-h**) in comparison to sunitinib. For a drug to be given orally, gastrointestinal absorption is critical pharmacokinetic behavior. As most patients prefer the oral route, therefore, estimation of gastrointestinal absorption is crucial in drug discovery processes.

The Brain Or IntestinaL EstimateD permeation method (BOILED-Egg) for estimating brain or intestinal permeation is a reliable predictor of both gastrointestinal absorption and brain permeation. BOILED Egg is a plot of polarity expressed in TPSA versus lipophilicity expressed in WLOGP. The yellow region (yolk) of the BOILED Egg plot represents the physicochemical space of compounds with highest opportunity for BBB permeability, while the white region (egg) represents the physicochemical space of compounds with highest probability of being passively absorbed by the gastrointestinal tract. The bioavailability radar is another model for rapid estimation of drug-likeness is which is a plot of six different physicochemical properties namely, size (SIZE), polarity (POLAR), lipophilicity (LIPO), solubility (INSOLU), flexibility (FLEX), and saturation (INSATU). The optimal range of each property is shown by the central pink hexagon (SIZE: MW between 150 and 500 g/mol, lipophilicity: XLOGP3 between −0.7 and +5.0, polarity: TPSA between 20 and 130$Å^2$, solubility: log S not higher than 6, saturation: fraction of carbons in the sp^3 hybridization not less than 0.25, and flexibility: no more than 9 rotatable bonds [79,80].

These calculations demonstrated that the target compounds **5a-h** have favorable parameters as compared to sunitinib which are presented in **Table 6**. As depicted in **table 6**, BOILED egg model **Figure 25** and bioavailability radar **Figure 26**, all target compounds were predicted to have high GI absorption as sunitinib. All target compounds obeyed Lipinski rule without deviation and had reasonable polarity (TPSA 78.51–108.05 $Å^2$) and credible molecular masses (below 500 g/mol). Only compound **5b** is predicted to pass through BBB but it is predicted be effluated outside of CNS by P-glycoprotein. Therefore, the synthesized compounds are promising anticancer lead compounds with favorable pharmacokinetic properties.

Table 4. Physicochemical properties of the synthesized compounds **5a-h** compared to sunitinib.

	5a	**5b**	**5c**	**5d**	**5e**	**5f**	**5g**	**5h**	**sunitinib**
Mwt	377.44	405.49	389.45	391.42	418.49	432.47	490.55	468.51	398.47
Fraction Csp3	0.23	0.29	0.26	0.23	0.29	0.25	0.33	0.19	0.36
Num. rotatable bonds	8	10	6	6	7	7	9	7	8
Num. H-bond acceptors	4	4	4	5	5	5	6	6	4
Num. H-bond donors	2	2	2	2	2	2	2	2	3
Molar Refractivity	113.01	122.63	119.62	115.90	131.24	131.44	147.37	142.26	116.31
TPSA	78.51	78.51	78.51	87.74	81.75	98.82	108.05	107.53	77.23
Log P	2.25	2.61	3.05	2.75	3.24	2.82	3.57	2.83	3.55
GI absorption	High	High	High	High	High	High	High	High	High
BBB penetration	No	Yes	No	No	No	No	No	No	Yes
Lipinski violation	0	0	0	0	0	0	0	0	0
Bioavailability score	0.55	0.55	0.55	0.55	0.55	0.55	0.55	0.55	0.55

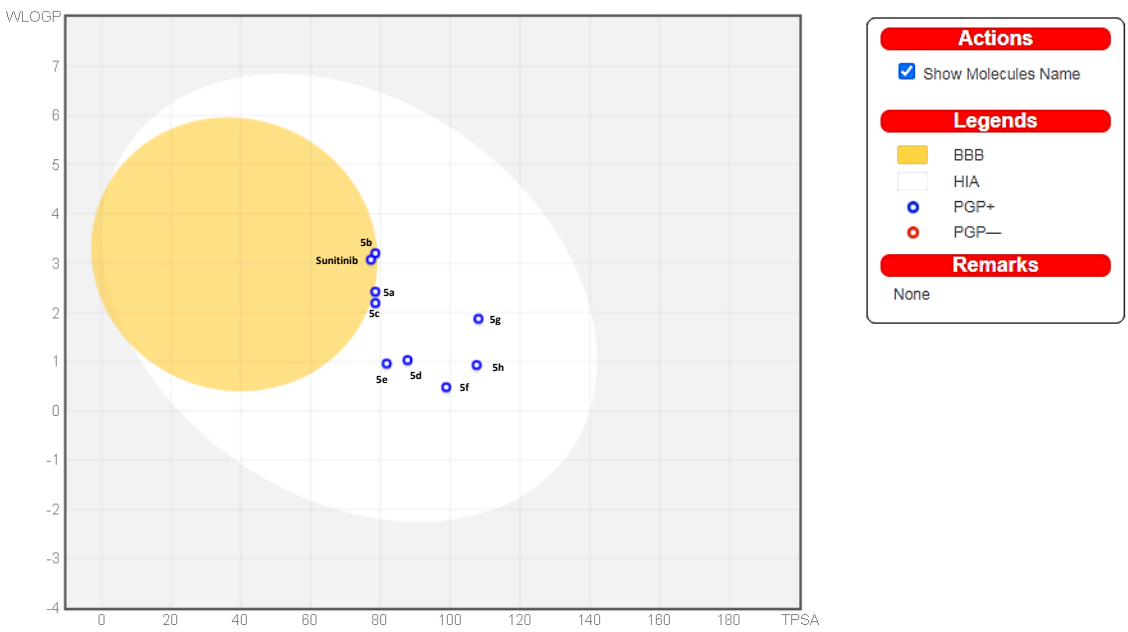

Figure 25: BOILED-Egg depiction of the synthesized compounds and sunitinib

Figure 26: Bioavailability radar of compounds **5b**,**5g** versus sunitinib.

Chapter (2)

5-chlorosalicylamide & 2-amino-5-phenyl-thiophen-3-carboxamide derivatives

2.1. Introduction

The fascinating bioactivity of 5-chlorosalicylamide derivatives was investigated, including antiviral, antibacterial, and anticancer activity. In order to treat human and animal tapeworm infections, niclosamide, a 5-chlorosalicylamide derivative, was first approved as an anthelmintic drug. It does this by interfering with mitochondrial metabolism [81] and oxidative phosphorylation uncoupling [82]. Studies in recent years have shown that niclosamide has anticancer properties against leukemia [83], breast cancer [84], and colorectal cancer [85]. Along with preventing mitochondrial uncoupling, niclosamide also interferes with numerous signaling pathways, including the Wnt/-catenin, mTORC1, STAT3, and NF-kB pathways [86]. In addition, niclosamide was reported to be effective in treatment of idiopathic pulmonary fibrosis (IPF) where, it ameliorated lung function and histopathological changes in bleomycin-challenged mice. Niclosamide blocked PI3K-mTORC1 signaling and halted the cell cycle to stop *in vitro* uncontrolled fibroblast growth. Furthermore, TGF-β-induced epithelial-mesenchymal transition (EMT) and ECM accumulation were reduced by niclosamide via the mTORC1-4EBP1 axis [87].

2-amino-5-phenylthiophen-3-carboxamide derivatives were reported to be effective against mycobacterium tuberculosis [88]. Moreover, 2-amino-5-phenylthiophen-3-carboxamide derivatives were found to be effective as IKKβ inhibitors. The inhibitor kappa B kinase β (IKKβ) is a serine-threonine protein kinase that is critically involved in the activation of the transcription factor

nuclear factor kappa B (NF-κB) in response to various inflammatory stimuli [89]. Nuclear Factor kappa B (NF-κB) is a pleiotropic transcription factor which regulates a set of genes responsible for both innate and adaptive immune responses [90,91]. Apart from its' vital role in immune modulation, NF-κB contributes a critical role in pathogenesis of many lung diseases including pulmonary fibrosis [92–94].

Motivated by the promising effects of 5-salicylamide derivatives and 2-amino-5-phenylthiophen-3-carboxamide on profibrogenic mediators, we attempted to design and synthesize new derivatives and determine their activity against collagen production and fibrosis.

2.2. Results and Discussion

2.2.1. Chemistry

Four 5-chlorosalicylamide derivatives were synthesized according as depicted in **scheme 2** through reaction of 5-chlorosalicylic acid **6** with substituted aniline **7** in super dehydrated toluene in presence of phosphorus trichloride to give compounds **8a-d**. All compounds were purified using column chromatography then their structures were confirmed using NMR and mass spectroscopy.

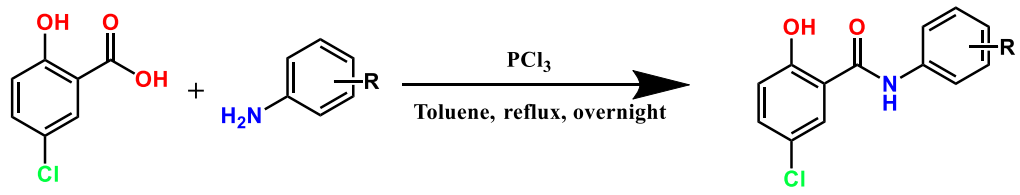

6 7 8a-d

8a: R= 3,5-Cl
8b: R= 4-CF_3
8c: R= 2,6-Cl-4-CF_3
8d: R= 3,5-Cl-4-CH_3

Scheme 2. Synthesis of the target compounds **8a-d**

Synthesis of 2-amino-5-phenylthiophen-3-carboxamide derivatives started with formation of thiophene ring through Gewald reaction by condensation of phenylacetaldehyde with α-cyanoacetamide in presence of elemental sulfur and morpholine. The formed 2-aminothiopene intermediate **11** was reacted with benzoyl chloride to give the amide derivative **13** in good yield. Moreover, urea derivatives **17a,b** were obtained via treatment of benzylamine or 2-aminomethylpyridine with the reactive phenyl carbamate **15** in super dehydrated DMSO. The phenyl carbamate intermediate **15** was synthesized through reaction of phenyl chloroformate with compound **11** in super dehydrated THF in presence of pyridine. Structure of the synthesized compounds were confirmed via NMR and mass spectroscopy.

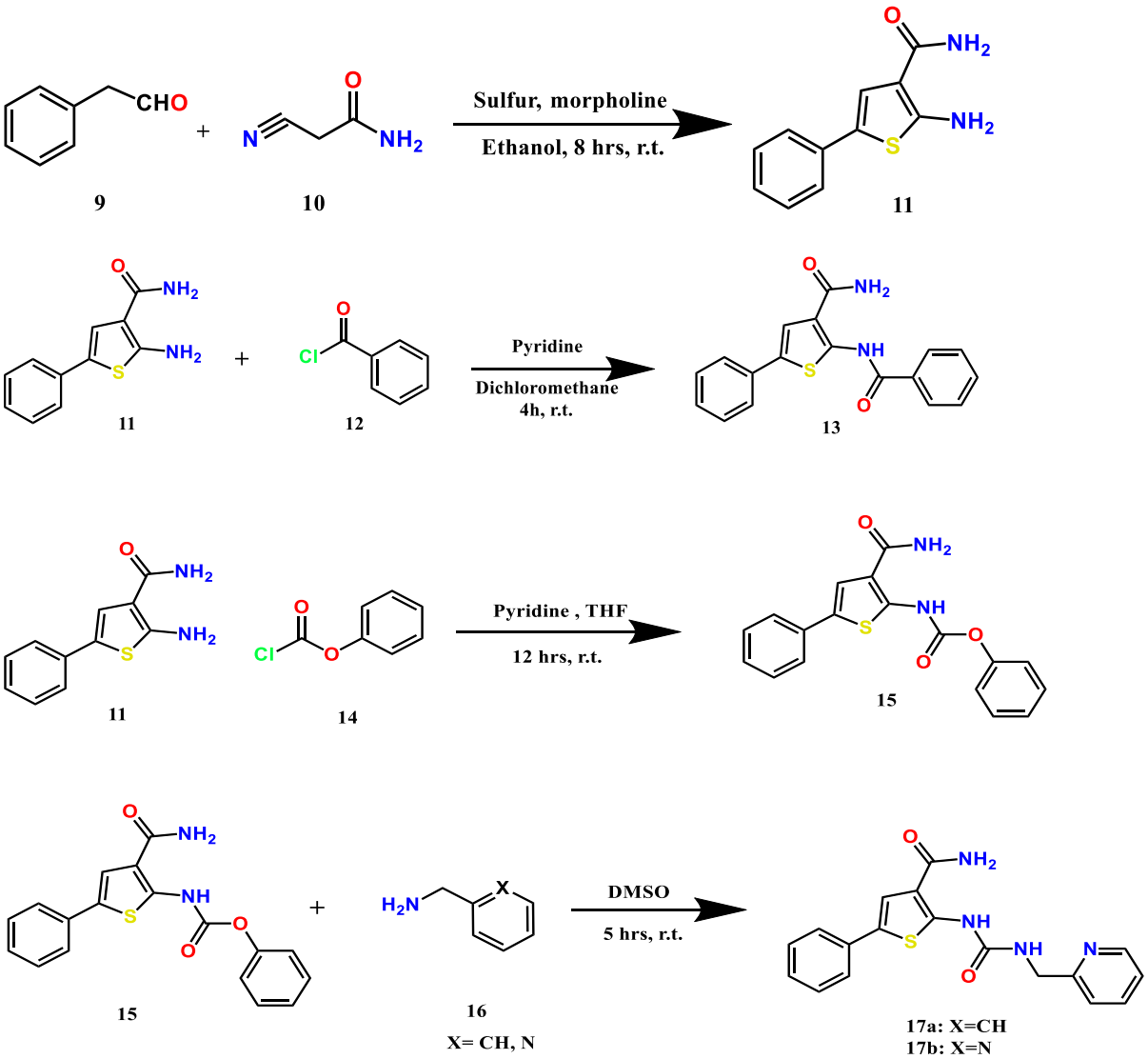

Scheme 3. Synthesis of the target compounds **13** and **17a,b**

2.2.2. Biology

All synthesized compounds (**8a-d, 13 and 17a,b**) were subjected for screening of antifibrosis activity through determination of effect on collagen production in human dermal fibroblasts stimulated with transforming growth factor-beta (TGF-β). The assay was held in comparison to DMSO as a negative control and HPH-15 as a positive control. HPH-15 is a promising compound developed by our group and reported to be effective in inhibition of skin fibrosis [37].

As depicted in **Figure 24**, the salicylamide derivatives **8a-d** revealed strong inhibitory effect on collagen production even more effective than HPH-15. But unfortunately, compounds **8a-d** demonstrated cytotoxic activity on the tested dermal fibroblasts. While 2-amino-5-phenylthiophen-3-carboxamide derivatives showed comparable activity to HPH-15 especially compound **17b** with 2-pyridylmethylurea moiety.

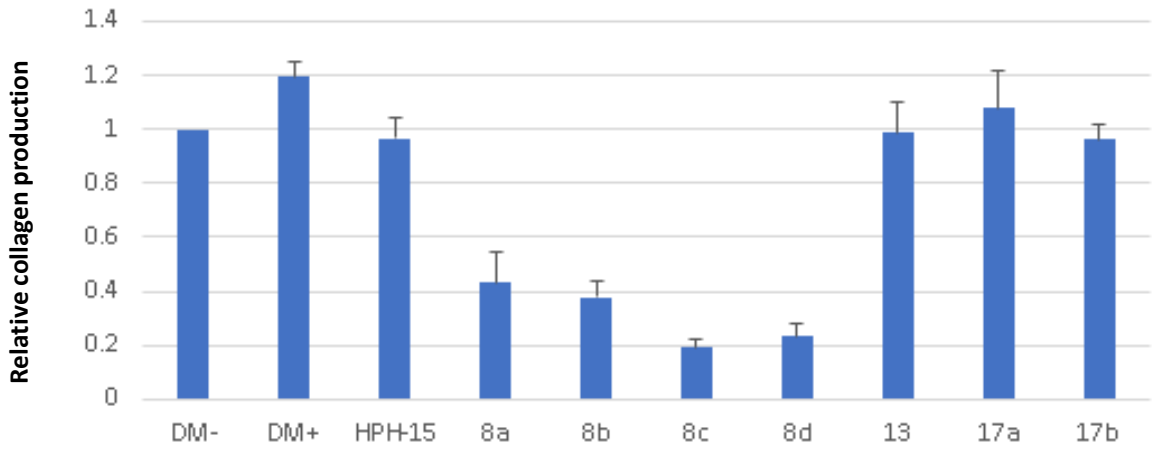

Figure 24: Effect of compounds **8a-d**, **13** and **17a,b** on production of collagen in human dermal fibroblasts.

Chapter (3)
Summary and Perspective

3.1 Summary

In the present thesis, a series of novel compounds based on iastin, 5-chlorosalicylic acid and 2-amino-5-phenylthiophen-3-carboxamide scaffolds were synthesized and evaluated for their anticancer and antifibrosis activity.

In chapter **1**, depending on the anticancer activity of isatin-based derivatives and α,β-unsaturated ketone moiety containing compounds, novel isatin derivatives containing α,β-unsaturated ketone moiety (**5a-h**) were synthesized. The compounds were submitted for screening of their cytotoxic activities against wide array of cancer cell lines in NCI. In the primary *in vitro* one dose antiproliferative assay compounds **5a-h** revealed potent cytotoxic activity against several cancer cell lines especially leukemia. Subsequently, the compounds were screened in 5 doses against HL-60 cell line and compounds **5a-h** depicted promising cytotoxic activity with IC_{50} values (0.38-2.57 µM). Intriguingly, an impressive safety profile for **5b** was reflected by a 37.2 times selectivity against HL-60 over PBMC. The effect of the most potent compounds **5b** and **5g** on apoptosis induction and cell cycle progression in HL-60 cells was evaluated. Both compounds induced apoptosis and demonstrated the ability to arrest cell cycle progression in G1 phase. Furtherly, the mechanism of action of compounds **5b** and **5g** was investigated in HL-60 cells. Compounds **5b** and **5g** was found to inhibit ERK1/2 phosphorylation and thus may be responsible for its effect on apoptosis and cell cycle progression. Concomitantly, *in silico* screening of **5b** and **5g** inside the active site of ERK2 (PDB ID: 6GDM) illustrated optimistic interactions with the key amino acid residues and comparable binding energy scores to the potent ERK1/2 inhibitor SCH772984

(native ligand). In addition, *In silico* calculation of pharmacokinetics and physicochemical properties revealed that the synthesized compounds possess good oral absorption and bioavailability. In conclusion, the synthesized compounds are stand out as strong chemotherapeutic agents that hold a clinical promise against several cancers especially acute myeloid leukemia

In chapter **2,** 5-chlorosalicylamide and 2-amino-5-phenylthiophen-3-carboxamide derivatives were reported to have effect on the fibrogenic mediators such as NF-kB. Therefore, some 5-chlorosalicylamide and 2-amino-5-phenylthiophen-3-carboxamide derivatives were synthesized and their structures were confirmed by NMR and HRMS. The synthesized compounds were subjected for screening of antifibrosis through detection of their effect on collagen production in normal human dermal fibroblasts cells line. The antifibrosis assay was carried out in comparison to HPH-15 which is reported to has good antifibrosis activity on skin fibrosis. Collagen production was induced by addition of TGF-β to cells. 5-chlorosalicylamide derivatives showed strong collagen production inhibition but demonstrated cytotoxicity to the used fibroblasts. While 2-amino-5-phenylthiophen-3-carboxamide derivatives, particularly **17-b** showed optimistic collagen production inhibitory activity which was comparable to HPH-15.

3.2 Perspective

Based on the obtained optimistic anticancer results of the synthesized isatin derivatives, we will continue synthesis of new isatin derivatives with different substitutions in order to reach to more potent compounds. The synthesized compounds will be screened against different cancer cell lines and the mechanism of action will be extensively investigated.

In addition, we will continue synthesis of new 2-amino-5-phenylthiophen-3-carboxamide derivatives. The synthesized compounds will be subjected for extensive antifibrosis studies and mechanistic elucidation.

Materials and Methods

General methods for synthesis

Chemistry

All glassware was oven-dried prior to use. Commercially available reagent-grade chemicals were used without further purification. The chemicals were purchased from Sigma-Aldrich (St. Louis, MO, USA), Kanto Chemical (Tokyo, Japan), Nacalai Tesque (Kyoto, Japan), Tokyo Chemical Industry (Tokyo, Japan), and FUJIFILM Wako (Osaka, Japan). The commercially available reagent-grade chemicals were used without further purification. The reaction progress was monitored by thin-layer chromatography (TLC) on TLC silica gel 60 F254 aluminum sheets (Merck, Darmstadt, Germany). The flash column chromatography was performed on Silica Gel 60N (40–100 mesh, Kanto Chemical). ^{1}H-NMR and ^{13}C-NMR spectra were recorded on a Bruker Avance 600 spectrometer (600 MHz) (Billerica, MA, USA). Mass spectrometry (MS) and high-resolution mass spectrometry (HRMS) data were recorded on a JEOL (Tokyo, Japan) JEOL JMS-700MStation using positive fast atom bombardment (FAB) technique with 3-nitrobenzyl alcohol as the matrix. Compound **11** was synthesized according to [88]

Synthesis of (*E*)-3-(2-(4-aminophenyl)-2-oxoethylidene)indolin-2-one (3b):

To a solution of **1** (3 g, 10 mmol, 1 equiv) in ethanol (20 mL), equivalent amount of *p*-aminoacetophenone **2** (2.75 g ,10 mmol, 1 equiv) and diethylamine (2 mL) were added. The mixture was stirred at room temperature overnight. The white precipitate formed was filtered and washed with ethanol and water. The obtained crude product was dissolved in ethanol (30 mL), conc. HCl (1 mL) was added, then the mixture was refluxed for 2 h. The mixture was cooled and poured to ice water. The reddish precipitate formed was collected by

filtration, washed with water. The crude product was purified was purified using column chromatography using hexane/ethyl acetate (1:1) as mobile phase.

Yield: 83%; reddish powder; ^{1}H-NMR (600 MHz, DMSO-d_6) δ 10.71 (s, 1H), 7.88 (d, *J* = 7.6 Hz, 1H), 7.81 – 7.77 (m, 2H), 7.61 (s, 1H), 7.29 (td, *J* = 7.7, 1.2 Hz, 1H), 6.91 (td, *J* = 7.6, 1.0 Hz, 1H), 6.88 – 6.84 (m, 1H), 6.65 – 6.61 (m, 2H), 6.39 (s, 2H). ^{13}C-NMR (150 MHz, DMSO-d_6) δ 187.97, 168.37, 154.79, 144.17, 134.08, 131.87, 131.36, 128.17, 126.35, 124.70, 121.53, 120.26, 112.95, 110.10.

Synthesis of (*E*)-2-chloro-*N*-(4-(2-(2-oxoindolin-3-ylidene)acetyl)phenyl) acetamide (4):

Chloroacetyl chloride (0.85 g, 7.5 mmol, 1 equiv) was added dropwise to a solution of **3b** (2g, 7.5 mmol, 1 equiv) and DIPEA (2 ml, 11.25 mmol, 1.5 equiv) in tetrahydrofurane (30 mL) at 0 ^{o}C. The mixture was stirred for 20 minutes at 0 ^{o}C and at room temperature for further 3 h. The reaction mixture was poured to ice water and the reddish precipitated formed was collected by filtration. The crude product was washed with hydrochloric acid (1M), then water. The crude product was purified by column chromatography using n-hexane/ethyl acetate (1:1) as mobile phase.

Yield: 72%; reddish powder; ^{1}H-NMR (600 MHz, DMSO-d_6) δ 10.79 (s, 1H), 10.74 (s, 1H), 8.14–8.05 (m, 2H), 8.11–8.08 (m, 2H), 7.99 (d, *J* = 7.7 Hz, 1H), 7.99 (d, *J* = 7.7 Hz, 1H), 7.88 – 7.77 (m, 2H), 7.83 – 7.80 (m, 2H), 7.71 (s, 1H), 7.71 (s, 1H), 7.34 (td, *J* = 7.7, 1.2 Hz, 1H), 7.34 (td, *J* = 7.7, 1.2 Hz, 1H), 6.95 (td, J = 7.7, 1.0 Hz, 1H), 6.95 (td, J = 7.7, 1.0 Hz, 1H), 6.91 – 6.87 (m, 1H), 6.90 – 6.88 (m, 1H), 4.33 (s, 2H). ^{13}C-NMR (150 MHz, DMSO-d_6) δ 189.77, 168.19, 165.32, 144.77, 143.59, 135.98, 132.70, 132.29, 130.13,

126.63, 126.22, 121.69, 119.99, 119.02, 110.31, 43.58. MS (FAB) m/z 378.3 $(M+H)^+$; HRMS (FAB) Calcd. for $C_{18}H_{14}N_2O_3Cl$: 341.0693, Found: 341.0707.

General procedure for synthesis of 5a-h:

Compound **4** (100 mg, 0.29 mmol, 1 equiv) with few crystals of potassium idide was dissolved in DMF (2 mL). The corresponding secondary amine (3.0 equiv) was added dropwise. The reaction mixture was stirred at room temperature for about 3 h. After the reaction monitored by TLC was over, brine was added to the reaction mixture under stirring, and the suspended mixture was filtered, washed with water. The crude residue was purified by column chromatography on silica gel to obtain the final products.

(*E*)-2-(diethylamino)-*N*-(4-(2-(2-oxoindolin-3-ylidene)acetyl)phenyl) acetamide (5a)

Mobile phase dichloromethane/methanol (99:1). Yield: 61%; reddish powder; ^{1}H-NMR (600 MHz, DMSO-d_6) δ 10.78 (s, 1H), 10.06 (s, 1H), 8.08–8.04 (m, 2H), 7.97 (d, *J* = 7.8 Hz, 1H), 7.91–7.86 (m, 2H), 7.70 (s, 1H), 7.33 (td, *J* = 7.7, 1.2 Hz, 1H), 6.94 (td, *J* = 7.7, 1.0 Hz, 1H), 6.88 (d, *J* = 7.7 Hz, 1H), 3.22 (s, 2H), 2.61 (q, *J* = 7.1 Hz, 4H), 1.02 (t, *J* = 7.1 Hz, 6H).^{13}C-NMR (150MHz, DMSO-d_6) δ 189.79, 170.75, 168.22, 144.71, 143.62, 135.85, 132.66, 131.91, 130.00, 126.58, 126.41, 121.70, 119.99, 118.98, 110.32, 57.38, 47.75, 11.88. MS (FAB) m/z 378.3 $(M + H)^+$; HRMS (FAB) Calcd. for $C_{22}H_{24}N_3O_3$: 378.1818. Found: 378.1809.

(*E*)-2-(dipropylamino)-*N*-(4-(2-(2-oxoindolin-3-ylidene)acetyl)phenyl) acetamide (5b)

Mobile phase dichloromethane/methanol (99:1). Yield: 63 %; reddish powder; ^{1}H-NMR (600 MHz, DMSO-d_6) δ 10.79 (s, 1H), 10.00 (s, 1H), 8.09–8.04 (m, 2H), 7.99 (dd, *J* = 7.8, 0.5 Hz, 1H), 7.87–7.84 (m, 2H), 7.71 (s, 1H),

7.34 (td, *J* = 7.7, 1.2 Hz, 1H), 6.95 (td, *J* = 7.7, 1.1 Hz, 1H), 6.90–6.87 (m, 1H), 3.25 (s, 2H), 1.48–1.43 (m, 4H), 0.87 (t, *J* = 7.4 Hz, 6H). ^{13}C-NMR (150 MHz, DMSO-d_6) δ 189.72, 170.60, 168.19, 144.75, 143.54, 135.89, 132.66, 131.93, 130.09, 126.61, 126.34, 121.67, 120.01, 118.76, 110.29, 58.38, 56.39, 19.85, 11.71. MS (FAB) m/z 406.4 $(M+H)^+$; HRMS (FAB) Calcd. for $C_{24}H_{28}N_3O_3$: 406.2131. Found: 406.2132.

(*E*)-*N*-(4-(2-(2-oxoindolin-3-ylidene)acetyl)phenyl)-2-(piperidin-1-yl) acetamide (5c)

Mobile phase dichloromethane/methanol (98:2). Yield: 57 %; reddish powder; ^{1}H-NMR (600 MHz, DMSO) δ 10.79 (s, 1H), 10.12 (s, 1H), 8.07 (d, *J* = 8.7 Hz, 2H), 7.99 (d, *J* = 7.7 Hz, 1H), 7.88 (d, *J* = 8.7 Hz, 2H), 7.71 (s, 1H), 7.34 (t, *J* = 7.6 Hz, 1H), 6.95 (t, *J* = 7.6 Hz, 1H), 6.89 (d, *J* = 7.8 Hz, 1H), 3.13 (s, 2H), 2.47 (s, 4H), 1.56 (dd, *J* = 10.7, 5.3 Hz, 4H), 1.40 (s, 2H).^{13}C-NMR (150 MHz, DMSO) δ 189.74, 169.41, 168.20, 144.75, 143.81, 135.88, 132.64, 131.88, 129.99, 126.62, 126.36, 121.67, 120.01, 118.98, 110.30, 62.65, 54.00, 25.40, 23.50. MS (FAB) m/z 390.3 $(M+H)^+$; HRMS (FAB) Calcd. for $C_{23}H_{23}N_3O_3$: 390.1818. Found: 390.1825.

(*E*)-2-morpholino-*N*-(4-(2-(2-oxoindolin-3-ylidene)acetyl)phenyl) acetamide (5d)

Mobile phase dichloromethane/methanol (98:2). Yield: 64%; reddish powder; ^{1}H-NMR (600 MHz, DMSO-d_6) δ 10.77 (s, 1H), 10.18 (s, 1H), 8.08–8.03 (m, 2H), 7.97 (d, *J* = 7.7 Hz, 1H), 7.88–7.84 (m, 2H), 7.70 (s, 1H), 7.33 (td, *J* = 7.7, 1.2 Hz, 1H), 6.94 (td, *J* = 7.7, 1.1 Hz, 1H), 6.90 – 6.87 (m, 1H), 3.65–3.62 (m, 4H), 3.19 (s, 2H), 2.53–2.51 (m, 4H). ^{13}C-NMR (150 MHz, DMSO-d_6) δ 189.78, 168.92, 168.21, 144.72, 143.81, 135.86, 132.66, 131.91, 129.98, 126.59, 126.38, 121.69, 120.00, 119.06, 110.31, 66.05, 62.02, 53.09.

MS (FAB) m/z 392.1 $(M+ H)^+$; HRMS (FAB) Calcd. for $C_{22}H_{22}N_3O_4$: 392.1610. Found: 392.1589.

(*E*)-2-(4-ethylpiperazin-1-yl)-*N*-(4-(2-(2-oxoindolin-3-ylidene)acetyl) phenyl)acetamide (5e)

Mobile phase dichloromethane/methanol (95:5). Yield: 62%; reddish powder; ^{1}H-NMR (600 MHz, DMSO-d_6) δ 10.81 (s, 1H), 10.16 (s, 1H), 8.10–8.05 (m, 2H), 8.04–8.00 (m, 1H), 7.89–7.86 (m, 2H), 7.72 (s, 1H), 7.34 (td, *J* = 7.7, 1.2 Hz, 1H), 6.96 (td, *J* = 7.7, 1.1 Hz, 1H), 6.92 – 6.89 (m, 1H), 3.58 (s, 4H), 3.20 (s, 2H), 2.57 (s, 4H), 2.40 (d, *J* = 7.2 Hz, 2H), 1.01 (t, *J* = 7.2 Hz, 3H). ^{13}C-NMR (150 MHz, DMSO-d_6) δ 189.68, 169.03, 168.22, 144.74, 143.78, 135.93, 132.65, 131.92, 129.98, 126.65, 126.26, 121.67, 120.01, 118.98, 110.29, 61.66, 52.41, 51.99, 51.47, 11.67. MS (FAB) m/z 419.2 $(M+H)^+$; HRMS (FAB) Calcd. for $C_{24}H_{27}N_4O_3$: 419.2083. Found: 419.2076.

(*E*)-2-(4-acetylpiperazin-1-yl)-*N*-(4-(2-(2-oxoindolin-3-ylidene)acetyl) phenyl)acetamide (5f)

Mobile phase dichloromethane/methanol (97:3). Yield: 60%; white solid; ^{1}H-NMR (600 MHz, DMSO-d_6) δ 10.79 (s, 1H), 10.23 (s, 1H), 8.07 (d, *J* = 8.8 Hz, 2H), 7.99 (d, *J* = 7.7 Hz, 1H), 7.88 (d, *J* = 8.8 Hz, 2H), 7.71 (s, 1H), 7.34 (td, *J* = 7.7, 1.0 Hz, 1H), 6.95 (td, *J* = 7.7, 0.7 Hz, 1H), 6.89 (d, *J* = 7.8 Hz, 1H), 3.50 (d, *J* = 4.3 Hz, 4H), 3.26 (s, 2H), 2.56 (s, 2H), 2.50 (s, 2H), 2.00 (s, 3H). ^{13}C-NMR (150 MHz, DMSO-d_6) δ 189.75, 168.20, 168.12, 144.75, 143.81, 135.89, 132.66, 131.93, 129.99, 126.62, 126.34, 121.68, 120.01, 119.06, 110.30, 61.36, 52.74, 52.31, 45.50, 40.67, 21.13. MS (FAB) m/z 433.1 $(M+ H)^+$; HRMS (FAB) Calcd. for $C_{24}H_{25}N_4O_4$: 433.1876. Found: 433.1890.

Tert-butyl (*E*)-4-(2-oxo-2-((4-(2-(2-oxoindolin-3-ylidene)acetyl)phenyl) amino)ethyl) piperazine-1-carboxylate (5g)

Mobile phase dichloromethane/methanol (99:1). Yield: 67%; reddish powder; ^{1}H-NMR (600 MHz, $CDCl_3$) δ 9.33 (s, 1H), 8.29 (d, *J* = 7.6 Hz, 1H), 8.23 (s, 1H), 8.14–8.10 (m, 2H), 7.84 (s, 1H), 7.75–7.72 (m, 2H), 7.31 (td, *J* = 7.7, 1.2 Hz, 1H), 7.01 (td, *J* = 7.7, 0.9 Hz, 1H), 6.86 (d, *J* = 7.7 Hz, 1H), 3.54 (s, 4H), 3.20 (s, 2H), 2.60 (s, 4H), 1.48 (s, 9H).^{13}C-NMR (150 MHz, $CDCl_3$) δ 189.58, 169.30, 168.42, 154.63, 143.25, 142.40, 136.49, 133.43, 132.64, 130.46, 128.06, 126.47, 122.87, 120.76, 118.98, 110.08, 80.21, 62.14, 53.34, 28.41. MS (FAB) m/z 491.2 $(M+H)^+$; HRMS (FAB) Calcd. for $C_{27}H_{31}N_4O_5$: 491.2294. Found: 491.2266.

(*E*)-*N*-(4-(2-(2-oxoindolin-3-ylidene)acetyl)phenyl)-2-(4-(pyrimidin-2-yl) piperazin-1-yl)acetamide (5h)

Mobile phase dichloromethane/methanol (99:1). Yield: 61%; reddish powder;^{1}H-NMR (600 MHz, DMSO-d_6) δ 10.78 (s, 1H), 10.23 (s, 1H), 8.36 (d, *J* = 4.7 Hz, 2H), 8.10–8.03 (m, 2H), 7.98 (dd, *J* = 7.7, 0.6 Hz, 1H), 7.91–7.85 (m, 2H), 7.70 (s, 1H), 7.33 (td, *J* = 7.7, 1.2 Hz, 1H), 6.95 (td, *J* = 7.6, 1.0 Hz, 1H), 6.90 – 6.86 (m, 1H), 6.63 (t, *J* = 4.7 Hz, 1H), 3.84 – 3.78 (m, 4H), 3.25 (s, 2H), 2.62 – 2.57 (m, 4H).^{13}C-NMR ^{13}C NMR (150 MHz, DMSO-d_6) δ 189.78, 169.04, 168.20, 161.21, 157.89, 144.74, 143.85, 135.87, 132.65, 131.92, 130.00, 126.60, 126.39, 121.68, 120.01, 119.07, 110.30, 110.09, 61.70, 52.41, 43.21. MS (FAB) m/z 469.2 $(M+H)^+$; HRMS (FAB) Calcd. for $C_{26}H_{25}N_6O_3$: 469.2006. Found: 469.2639.

General method for synthesis of compound 8a-d

A mixture of 5-chlorosalicylic acid **6** (173mg, l mmol, 1 equiv), substituted aniline **7** (l mmol, 1 equiv), and phosphorus trichloride (44 μL, 0.5mmol) in toluene (5mL) was refluxed overnight under argon atmosphere.

The reaction mixture was cooled then evaporated under vacuum. The residue was dissolved in ethyl acetate (50 ml) then washed with sodium bicarbonate 10% (30 ml), then 1N HCl (30 ml) and finally brine (30 ml). The organic layer was dried over anhydrous sodium sulfate, then evaporated under vacuum. The obtained residue was purified using column chromatography on silica gel (n-hexane/ethyl acetate: 2/l) to give the title compound.

5-chloro-*N*-(3,5-dichlorophenyl)-2-hydroxybenzamide (8a)

Yield: 56%, white powder, ^{1}H-NMR (600 MHz, DMSO-d_6) δ 11.48 (s, 1H), 10.58 (s, 1H), 7.84 (dd, *J* = 2.2, 1.3 Hz, 3H), 7.48 (dd, *J* = 8.8, 2.7 Hz, 1H), 7.37 (t, *J* = 1.8 Hz, 1H), 7.04 (d, *J* = 8.8 Hz, 1H). ^{13}C NMR (150 MHz, DMSO-d_6) δ 165.07, 156.17, 140.60, 134.03, 133.09, 128.55, 123.28, 122.78, 120.26, 118.99, 118.63. MS (FAB) m/z 316 $(M+H)^+$.

5-chloro-2-hydroxy-*N*-(4-(trifluoromethyl)phenyl)benzamide (8b)

Yield: 58%, white powder, ^{1}H-NMR (600 MHz, DMSO-d_6) δ 11.60 (s, 1H), 10.66 (s, 1H), 7.95 (d, *J* = 8.5 Hz, 2H), 7.90 (d, *J* = 2.7 Hz, 1H), 7.75 (d, *J* = 8.5 Hz, 2H), 7.49 (dd, *J* = 8.8, 2.7 Hz, 1H), 7.04 (d, *J* = 8.8 Hz, 1H). ^{13}C-NMR (151 MHz, DMSO- d_6) δ 165.07, 156.28, 141.82, 133.05, 128.60, 126.02 (q, *J* = 3.7 Hz), 125.19, 123.40, 122.80, 120.46, 120.27, 119.00. MS (FAB) m/z 316 $(M+H)^+$.

5-chloro-*N*-(2,6-dichloro-4-(trifluoromethyl)phenyl)-2-hydroxybenzamide (8c)

Yield: 43%, white powder, ^{1}H-NMR (600 MHz, $CDCl_3$) δ 11.30 (s, 1H), 7.75 (s, 1H), 7.71 (s, 2H), 7.63 (d, *J* = 2.5 Hz, 1H), 7.46 (dd, *J* = 8.9, 2.5 Hz, 1H), 7.02 (d, *J* = 8.9 Hz, 1H). ^{13}C-NMR (150 MHz, $CDCl_3$) δ 167.34, 160.47, 135.47, 134.35, 131.43, 125.85, 125.78 (q, *J* = 3.7 Hz), 124.10, 123.25,

121.44, 120.56, 114.35. MS (FAB) m/z 384.2 $(M+H)^+$; HRMS (FAB) Calcd. for $C_{14}H_8NO_2Cl_3F_3$: 383.9573. Found: 383.9595.

5-chloro-*N*-(3,5-dichloro-4-methylphenyl)-2-hydroxybenzamide (8d)

Yield: 52%, white powder, ^{1}H-NMR (600 MHz, DMSO- d_6) δ 11.56 (s, 1H), 10.51 (s, 1H), 7.90 – 7.82 (m, 3H), 7.48 (dd, *J* = 8.8, 2.7 Hz, 1H), 7.03 (d, *J* = 8.8 Hz, 1H), 2.39 (s, 3H). ^{13}C NMR (150 MHz, DMSO- d_6) δ 165.07, 156.40, 137.50, 134.23, 133.11, 128.74, 128.45, 122.73, 119.97, 119.58, 119.04, 16.60. ^{13}C NMR (150 MHz, DMSO) δ 165.07, 156.40, 137.50, 134.23, 133.11, 128.74, 128.45, 122.73, 119.97, 119.58, 119.04, 16.60. MS (FAB) m/z 329 $(M+H)^+$; HRMS (FAB) Calcd. for $C_{14}H_{10}NO_2Cl_3$: 328.9777. Found: 328.9710.

Synthesis of 2-benzamido-5-phenylthiophene-3-carboxamide (13)

Benzoyl chloride **12** (1.5 equiv) was added to a solution of **11** (200 mg, 1 equiv) and pyridine (3 equiv) in THF (5 ml) at 0 ^{o}C. The reaction mixture was stirred at room temperature for 6 hrs. Ethyl acetate (30 ml) was added to the reaction mixture then extracted with sodium bicarbonate (30 ml), then brine (30 ml). The organic layer was dried using anhydrous sodium sulfate then evaporated under vacuum. The residue was dissolved in 5 ml ethyl acetate then diethyl ether (10 ml) was added, and the resulting powder was filtered and washed with diethyl ether (20 ml).

Yield: 74%, white powder, ^{1}H-NMR (600 MHz, DMSO-d_6) δ 13.46 (s, 1H), 8.11 (s, 1H), 7.97 (s, 2H), 7.95 (d, *J* = 1.4 Hz, 1H), 7.77 (s, 1H), 7.73 – 7.70 (m, 1H), 7.67 – 7.62 (m, 4H), 7.48 – 7.45 (m, 2H), 7.35 – 7.32 (m, 1H). ^{13}C-NMR (150 MHz, DMSO-d_6) δ 167.23, 162.52, 145.50, 133.53, 132.83, 132.28, 131.92, 129.26, 127.42, 127.05, 124.79, 121.22, 119.53, 116.63. MS (FAB) m/z 323 $(M+H)^+$**.**

Synthesis of phenyl (3-carbamoyl-5-phenylthiophen-2-yl)carbamate (15)

Phenyl chloroformate (0.5 ml, 3.95 mmol, 1.1 equiv) was added dropwise to a solution of **11** (0.784 g, 3.59 mmol, 1 equiv) and pyridine (0.36 ml, 3.95 mmol, 4.48 equiv) in THF (15 ml) at 0°C under argon atmosphere. The reaction mixture was stirred for 15 minutes at 0°C and for further 1.5 h at room temperature. Water (50 ml) was added to the reaction mixture and the resulting turbid solution was extracted 3 times with ethyl acetate (30 ml). The combined organic layers were washed with brine then dried over anhydrous sodium sulfate and evaporated under vacuum. The residue was purified using column chromatography and dichloromethane/methanol (19:1) as mobile phase.

Yield: 91%; Pale yellow powder; ^{1}H-NMR (600 MHz, DMSO-d_6) δ 11.99 (s, 1H), 8.03 (s, 1H), 7.91 (s, 1H), 7.76 (s, 1H), 7.59 – 7.55 (m, 2H), 7.48 – 7.42 (m, 4H), 7.34 – 7.29 (m, 4H). ^{13}C-NMR (150 MHz, DMSO-d_6) δ 166.84, 150.18, 146.28, 133.30, 131.82, 129.54, 129.33, 129.22, 127.42, 126.09, 124.64, 121.66, 115.93, 115.22. MS (FAB) m/z 338.1 $(M+H)^+$; HRMS (FAB) Calcd. for $C_{18}H_{14}N_2O_3S$: 338.0725. Found: 338.0725.

General procedure for synthesis of compounds 17a,b

The respective amine **16** (1.48 mmol, 2.5 equiv) was added to a solution of **15** (0.2 g, 0.59 mmol, 1 equiv) in DMSO (2 ml) at room temperature for 6h. Water (30 ml) was added to the reaction and the resulting turbid solution was extracted three times with ethyl acetate (20 ml). The combined organic layers were washed with brine then dried over anhydrous sodium sulfate and evaporated under vacuum. The residue was purified using column chromatography and dichloromethane/methanol (18:2) as mobile phase.

2-(3-benzylureido)-5-phenylthiophene-3-carboxamide (17a)

Yield: 61%; Pale yellow powder; ^{1}H-NMR (600 MHz, DMSO- d_6) δ 11.20 (s, 1H), 8.43 (s, 1H), 7.78 (s, 1H), 7.76 (s, 1H), 7.53 (d, *J* = 7.0 Hz, 2H), 7.41 – 7.25 (m, 10H), 4.32 (d, *J* = 4.5 Hz, 2H). ^{13}C NMR (150 MHz, DMSO-d_6) δ 166.86, 153.66, 148.64, 139.62, 134.06, 129.52, 129.06, 128.31, 127.25, 126.84, 126.68, 124.29, 119.48, 113.12, 43.13, 43.07. MS (FAB) m/z 352 $(M+H)^+$.

5-phenyl-2-(3-(pyridin-2-ylmethyl)ureido)thiophene-3-carboxamide (17b)

Yield: 65%; Pale yellow powder; ^{1}H-NMR (600 MHz, DMSO-d_6) δ 11.26 (s, 1H), 8.61 – 8.44 (m, 2H), 7.82 – 7.70 (m, 3H), 7.55 – 7.49 (m, 2H), 7.42 – 7.33 (m, 4H), 7.30 – 7.22 (m, 2H), 4.42 (d, *J* = 5.9 Hz, 2H, ^{13}C-NMR (150 MHz, DMSO) δ 166.83, 158.81, 153.80, 148.87, 148.59, 136.74, 134.06, 129.57, 129.07, 126.69, 124.29, 122.12, 120.99, 119.43, 113.21, 45.05. MS (FAB) m/z 375.1 $(M+Na)^+$; HRMS (FAB) Calcd. for $C_{18}H_{16}N_4O_2SNa$: 375.0892. Found: 375.0880.

Biology

a) Evaluation of *in vitro* antiproliferative activity for compounds by NCI

The methodology of the NCI anticancer screening has been described in detail elsewhere (http://www.dtp.nci.nih.gov). Primary anticancer assay was performed at approximately 60 human tumor cell lines panel derived from nine neoplastic diseases, in accordance with the protocol of the Drug Evaluation Branch, National Cancer Institute, Bethesda, USA [69].

b) Evaluation of antiproliferative activity for compounds against HL-60

The synthesized compounds and staurosporine (AdipoGen Life Sciences, San Diego, CA, USA) were dissolved in dimethyl sulfoxide (DMSO)

(FUJIFILM-Wako, Osaka, Japan), and the solution was added to the cell-culture medium at a 1:100 volume. The human promyelocytic leukemia cells line HL-60 (provided by the RIKEN BRC through the National Bio-Resource Project of the MEXT/AMED, Japan (RCB0041 and RCB1904)) was maintained in RPMI-1640 supplemented with 10% heat-inactivated fetal bovine serum (FBS) (Capricorn Scientific, Ebsdorfergrund, Germany), 89 μg/mL of streptomycin (Meiji Seika Pharma, Tokyo, Japan), and 2.0 μg/mL of amphotericin B (Clinigen, Burton-on-Trent, UK). To suspended HL-60 cells, chemicals were immediately added. At 2 d post-addition, MTT assay was performed to evaluate cell viability as previously described [95]. IC_{50} was calculated using GraphPad Prism 9.4.1.

c) Cell cycle analysis and apoptosis analysis

HL-60 cells were plated at $8x10^4$ cells on a 35 mm dish (Sumitomo Bakelite, Tokyo, Japan), and chemicals were added. To observe cell cycle, the cells were incubated for 1 d, and washed with PBS (500 μL) followed by incubation with Cell Cycle Assay Solution Deep Red (Dojindo, Kumamoto, Japan) at 37 ℃ for 15 min. Fluorescence signal was detected in FL4 using flow cytometer BD FACSCalibur (BD Biosciences, Franklin Lakes, NJ, USA). For apoptosis/necrosis assay, the cells were incubated for 0.5-1 d, and washed with PBS followed by incubation with annexin binding buffer containing Annexin-V-FITC (MBL Life Science, Tokyo, Japan) and 7-Aminoactinomycin D (7-AAD) (BD Biosciences) at room temperature for 15 min. Fluorescence signal of FITC and 7-AAD were detected in FL1 and FL3, respectively using flow cytometer BD FACSCalibur.

d) Western blot

For the analysis of signaling pathways, FBS-free medium was used to culture cells. Cells were lysed using a RIPA buffer (50 mM Tris-HCl (pH 7.8),

150 mM NaCl, 1% Nonidet P-40, 0.5% sodium deoxycholate, 1% protease inhibitor cocktail (Nacalai Tesque, Kyoto, Japan), 1% phosphatase inhibitor cocktail (Nacalai Tesque)), and the protein concentration of the lysate was determined using a BCA Protein Assay Kit (Thermo Fisher Scientific). Gel electrophoresis and immunoblotting were performed using 10 μg total protein per well. As an antibody, Phospho-p44/42 MAPK (Erk1/2) (Thr202/Tyr204) (D13.14.4E) XP® Rabbit mAb (Cell Signaling Technology) or anti-β-actin (AC-15) (Sigma–Aldrich), was used. Immunoreactivity was detected by chemiluminescence using an ImmunoStar LD (FUJIFILM Wako).

e) Antifibrosis assay

1. Chemicals in biological experiments

The synthesized compounds were dissolved in dimethyl sulfoxide (DMSO) (FUJIFILM-Wako, Osaka, Japan), and the solution was added to the cell-culture medium at a 1:200 volume. TGF-β1 was purchased from R&D Systems (Minneapolis, MN, USA), and used as TGF-β.

2. Cells

The normal human dermal fibroblasts cells line (purchased from Lonza) was maintained in Fibroblast Growth Medium 2 (Takara), 89 μg/mL of streptomycin (Meiji Seika Pharma, Tokyo, Japan), and 2.0 μg/mL of amphotericin B (Clinigen, Burton-on-Trent, UK).

3. Collagen detection assay

The cells were plated at $1x10^6$ cells on a 6-well cell culture plate (AS ONE, Osaka, Japan) and cultured overnight. Chemicals were added to the cells for 1 h, followed by the addition of TGF-β. After incubating the cells for 3 d, cells were fixed with MeOH for 15 min and washed with PBS three times. The cells were then incubated with PBS containing 1% BSA (Nacalai) for 30 min at 4℃, and reacted with the anti-Collagen I (Southern Biotechnology

Associates Inc.) in PBS for 5 h. After washing with PBS three times, the cells were reacted with rabbit anti-goat IgG (H+L) (Proteintech Group) in PBS for 30 min. The cells were washed with PBS three times and reacted with OPD (Wako) for 30 min and measured the absorbance at 450 nm using microplate reader CYTATION 5 (BioTec).

In silico screening

a) Molecular docking

The 3D X-ray crystal structure of ERK2 co-crystalized with SCH772984 was downloaded from the protein data bank, PDB, (PDB ID: 6GDM). Docking of the target ligands as a conformations database was performed inside SCH772984 binding site using MOE 2019 as described before. A scoring function, London dG, was employed for comparison of different conformers, poses with lower values are more beneficial. Re-docking of the native ligand SCH772984 on the active site of ERK (PDB ID: 6GDM) was performed for docking protocol validation.

b) Prediction of physicochemical properties and pharmacokinetics

The physicochemical and pharmacokinetic properties of compounds (**5a-h**) and sunitinib were estimated by SwissADME web tool [79,80].

Reference

[1] C.M. Croce, Oncogenes and cancer, N Engl J Med. 358 (2008) 502–511. https://doi.org/10.1056/NEJMRA072367.

[2] A. Sudhakar, History of Cancer, Ancient and Modern Treatment Methods, J Cancer Sci Ther. 1 (2009) i–iv. https://doi.org/10.4172/1948-5956.100000E2.

[3] K.M.B.S.S.V.M.A. Saini A, Cancer causes and treatments, Int J Pharm Sci Res. 11 (2020) 3109–3122.

[4] A. Leitch, A British Medical Association Lecture ON GALL STONES AND CANCER OF THE GALL BLADDER: AN EXPERIMENTAL STUDY, BMJ. 2 (1924) 451–454. https://doi.org/10.1136/bmj.2.3324.451.

[5] V.T. DeVita, E. Chu, A History of Cancer Chemotherapy, Cancer Res. 68 (2008) 8643–8653. https://doi.org/10.1158/0008-5472.CAN-07-6611.

[6] C. Pottier, M. Fresnais, M. Gilon, G. Jérusalem, R. Longuespée, N.E. Sounni, Tyrosine Kinase Inhibitors in Cancer: Breakthrough and Challenges of Targeted Therapy, Cancers (Basel). 12 (2020) 731. https://doi.org/10.3390/cancers12030731.

[7] A.M. Kidger, J. Sipthorp, S.J. Cook, ERK1/2 inhibitors: New weapons to inhibit the RAS-regulated RAF-MEK1/2-ERK1/2 pathway, Pharmacol Ther. 187 (2018) 45–60. https://doi.org/10.1016/j.pharmthera.2018.02.007.

[8] Y. Lu, B. Liu, Y. Liu, X. Yu, G. Cheng, Dual effects of active ERK in cancer: A potential target for enhancing radiosensitivity (Review), Oncol Lett. 20 (2020) 993–1000. https://doi.org/10.3892/ol.2020.11684.

[9] R.M. Sammons, R. Ghose, K.Y. Tsai, K.N. Dalby, Targeting ERK beyond the boundaries of the kinase active site in melanoma, Mol Carcinog. 58 (2019) 1551–1570. https://doi.org/10.1002/mc.23047.

[10] N.Y. Al-Madhoun, S.Z. Gadhoum, J.S. Merzaban, ERK1/2 Pathway Is Required for Differentiation of AML Triggered by Anti-CD44 Monoclonal Antibodies, Blood. 120 (2012) 4334–4334. https://doi.org/10.1182/blood.V120.21.4334.4334.

[11] T.D. Heightman, V. Berdini, H. Braithwaite, I.M. Buck, M. Cassidy, J. Castro, A. Courtin, J.E.H. Day, C. East, L. Fazal, B. Graham, C.M. Griffiths-Jones, J.F. Lyons, V. Martins, S. Muench, J.M. Munck, D. Norton, M. O'Reilly, N. Palmer, P. Pathuri, M. Reader, D.C. Rees, S.J. Rich, C. Richardson, H. Saini, N.T. Thompson, N.G. Wallis, H. Walton, N.E. Wilsher, A.J.-A. Woolford, M. Cooke, D. Cousin, S. Onions, J. Shannon, J. Watts, C.W. Murray, Fragment-Based Discovery of a Potent, Orally Bioavailable Inhibitor That Modulates the Phosphorylation and Catalytic Activity of ERK1/2, J Med Chem. 61 (2018) 4978–4992. https://doi.org/10.1021/acs.jmedchem.8b00421.

[12] X. Pan, J. Pei, A. Wang, W. Shuai, L. Feng, F. Bu, Y. Zhu, L. Zhang, G. Wang, L. Ouyang, Development of small molecule extracellular signal-regulated kinases (ERKs) inhibitors for cancer therapy, Acta Pharm Sin B. 12 (2022) 2171–2192. https://doi.org/10.1016/j.apsb.2021.12.022.

[13] R. Bataller, D.A. Brenner, Liver fibrosis, Journal of Clinical Investigation. 115 (2005) 209–218. https://doi.org/10.1172/JCI24282.

[14] T.A. Wynn, T.R. Ramalingam, Mechanisms of fibrosis: therapeutic translation for fibrotic disease, Nat Med. 18 (2012) 1028–1040. https://doi.org/10.1038/nm.2807.

[15] T.A. Wynn, Integrating mechanisms of pulmonary fibrosis, Journal of Experimental Medicine. 208 (2011) 1339–1350. https://doi.org/10.1084/jem.20110551.

[16] D.C. Rockey, P.D. Bell, J.A. Hill, Fibrosis — A Common Pathway to Organ Injury and Failure, New England Journal of Medicine. 372 (2015) 1138–1149. https://doi.org/10.1056/NEJMra1300575.

[17] T. Wynn, Cellular and molecular mechanisms of fibrosis, J Pathol. 214 (2008) 199–210. https://doi.org/10.1002/path.2277.

[18] H. Kawano, J. Kimura-Kuroda, Y. Komuta, N. Yoshioka, H.P. Li, K. Kawamura, Y. Li, G. Raisman, Role of the lesion scar in the response to damage and repair of the central nervous system, Cell Tissue Res. 349 (2012) 169–180. https://doi.org/10.1007/s00441-012-1336-5.

[19] X. Li, L. Zhu, B. Wang, M. Yuan, R. Zhu, Drugs and Targets in Fibrosis, Front Pharmacol. 8 (2017). https://doi.org/10.3389/fphar.2017.00855.

[20] K.M. Mortimer, D.B. Bartels, N. Hartmann, J. Capapey, J. Yang, R. Gately, C. Enger, Characterizing Health Outcomes in Idiopathic Pulmonary Fibrosis using US Health Claims Data, Respiration. 99 (2020) 108–118. https://doi.org/10.1159/000504630.

[21] T.M. Maher, E. Bendstrup, L. Dron, J. Langley, G. Smith, J.M. Khalid, H. Patel, M. Kreuter, Global incidence and prevalence of idiopathic pulmonary fibrosis, Respir Res. 22 (2021) 197. https://doi.org/10.1186/s12931-021-01791-z.

[22] S.C. Schäfer, M. Funke-Chambour, S. Berezowska, Idiopathische Lungenfibrose – Epidemiologie, Ursachen und klinischer Verlauf, Pathologe. 41 (2020) 46–51. https://doi.org/10.1007/s00292-019-00747-x.

[23] D.S. Glass, D. Grossfeld, H.A. Renna, P. Agarwala, P. Spiegler, L.J. Kasselman, A.D. Glass, J. DeLeon, A.B. Reiss, Idiopathic pulmonary fibrosis: Molecular mechanisms and potential treatment approaches, Respir Investig. 58 (2020) 320–335. https://doi.org/10.1016/j.resinv.2020.04.002.

[24] F.J. Martinez, H.R. Collard, A. Pardo, G. Raghu, L. Richeldi, M. Selman, J.J. Swigris, H. Taniguchi, A.U. Wells, Idiopathic pulmonary fibrosis, Nat Rev Dis Primers. 3 (2017) 1–19. https://doi.org/10.1038/nrdp.2017.74.

[25] Q. Mei, Z. Liu, H. Zuo, Z. Yang, J. Qu, Idiopathic Pulmonary Fibrosis: An Update on Pathogenesis, Front Pharmacol. 12 (2022) 1–14. https://doi.org/10.3389/fphar.2021.797292.

[26] S.L. Friedman, Liver fibrosis – from bench to bedside, J Hepatol. 38 (2003) 38–53. https://doi.org/10.1016/S0168-8278(02)00429-4.

[27] P. Ginès, A. Cárdenas, V. Arroyo, J. Rodés, Management of Cirrhosis and Ascites, New England Journal of Medicine. 350 (2004) 1646–1654. https://doi.org/10.1056/NEJMra035021.

[28] R. Bataller, D.A. Brenner, Hepatic Stellate Cells as a Target for the Treatment of Liver Fibrosis, Semin Liver Dis. 21 (2001) 437–452. https://doi.org/10.1055/s-2001-17558.

[29] L.A. Murtha, M.J. Schuliga, N.S. Mabotuwana, S.A. Hardy, D.W. Waters, J.K. Burgess, D.A. Knight, A.J. Boyle, The Processes and Mechanisms of Cardiac and Pulmonary Fibrosis, Front Physiol. 8 (2017) 1–15. https://doi.org/10.3389/fphys.2017.00777.

[30] D. Mozaffarian, E.J. Benjamin, A.S. Go, D.K. Arnett, M.J. Blaha, M. Cushman, S.R. Das, S. de Ferranti, J.-P. Després, H.J. Fullerton, V.J. Howard, M.D. Huffman, C.R. Isasi, M.C. Jiménez, S.E. Judd, B.M. Kissela, J.H. Lichtman, L.D. Lisabeth, S. Liu, R.H. Mackey, D.J. Magid, D.K. McGuire, E.R. Mohler, C.S. Moy, P. Muntner, M.E. Mussolino, K. Nasir, R.W. Neumar, G. Nichol, L. Palaniappan, D.K. Pandey, M.J. Reeves, C.J. Rodriguez, W. Rosamond, P.D. Sorlie, J. Stein, A. Towfighi, T.N. Turan, S.S. Virani, D. Woo, R.W. Yeh, M.B. Turner, Heart Disease and Stroke Statistics—2016 Update, Circulation. 133 (2016) e38-360. https://doi.org/10.1161/CIR.0000000000000350.

[31] C. Jellis, J. Martin, J. Narula, T.H. Marwick, Assessment of Nonischemic Myocardial Fibrosis, J Am Coll Cardiol. 56 (2010) 89–97. https://doi.org/10.1016/j.jacc.2010.02.047.

[32] M. Disertori, M. Masè, F. Ravelli, Myocardial fibrosis predicts ventricular tachyarrhythmias, Trends Cardiovasc Med. 27 (2017) 363–372. https://doi.org/10.1016/j.tcm.2017.01.011.

[33] S. Hinderer, K. Schenke-Layland, Cardiac fibrosis – A short review of causes and therapeutic strategies, Adv Drug Deliv Rev. 146 (2019) 77–82. https://doi.org/10.1016/j.addr.2019.05.011.

[34] G. ERTL, S. FRANTZ, Healing after myocardial infarction, Cardiovasc Res. 66 (2005) 22–32. https://doi.org/10.1016/j.cardiores.2005.01.011.

[35] J. Neefs, N.W.E. van den Berg, J. Limpens, W.R. Berger, S.M. Boekholdt, P. Sanders, J.R. de Groot, Aldosterone Pathway Blockade to Prevent Atrial Fibrillation: A Systematic Review and Meta-Analysis, Int J Cardiol. 231 (2017) 155–161. https://doi.org/10.1016/j.ijcard.2016.12.029.

[36] M. BUJAK, N. FRANGOGIANNIS, The role of TGF-β signaling in myocardial infarction and cardiac remodeling, Cardiovasc Res. 74 (2007) 184–195. https://doi.org/10.1016/j.cardiores.2006.10.002.

[37] V.H. Luong, T. Chino, N. Oyama, T. Matsushita, Y. Sasaki, D. Ogura, S. Niwa, T. Biswas, A. Hamasaki, M. Fujita, Y. Okamoto, M. Otsuka, H. Ihn, M. Hasegawa, Blockade of TGF-β/Smad signaling by the small compound HPH-15 ameliorates experimental skin fibrosis, Arthritis Res Ther. 20 (2018) 46. https://doi.org/10.1186/s13075-018-1534-y.

[38] V. Varun, S. Sonam, R. Kakkar, Isatin and its derivatives: a survey of recent syntheses, reactions, and applications, Medchemcomm. 10 (2019) 351–368. https://doi.org/10.1039/C8MD00585K.

[39] A. Medvedev, O. Buneeva, O. Gnedenko, V. Fedchenko, M. Medvedeva, Y. Ivanov, V. Glover, M. Sandler, Isatin interaction with glyceraldehyde-3-phosphate dehydrogenase, a putative target of neuroprotective drugs: partial agonism with deprenyl, in: Oxidative Stress and Neuroprotection, Springer Vienna, Vienna, n.d.: pp. 97–103. https://doi.org/10.1007/978-3-211-33328-0_11.

[40] A. Andreani, S. Burnelli, M. Granaiola, A. Leoni, A. Locatelli, R. Morigi, M. Rambaldi, L. Varoli, M.A. Cremonini, G. Placucci, New isatin derivatives with antioxidant activity, Eur J Med Chem. 45 (2010) 1374–1378. https://doi.org/10.1016/j.ejmech.2009.12.035.

[41] K. Khan, U. Mughal, A. Khan, F. Naz, S. Perveen, M. Choudhary, N-Aroylated Isatins: Antiglycation Activity, Lett Drug Des Discov. 7 (2010) 188–193. https://doi.org/10.2174/157018010790596597.

[42] I. Chiyanzu, C. Clarkson, P.J. Smith, J. Lehman, J. Gut, P.J. Rosenthal, K. Chibale, Design, synthesis and anti-plasmodial evaluation in vitro of new 4-aminoquinoline isatin derivatives, Bioorg Med Chem. 13 (2005) 3249–3261. https://doi.org/10.1016/j.bmc.2005.02.037.

[43] P.K. Sharma, S. Balwani, D. Mathur, S. Malhotra, B.K. Singh, A.K. Prasad, C. Len, E. v. van der Eycken, B. Ghosh, N.G.J. Richards, V.S. Parmar, Synthesis and anti-inflammatory activity evaluation of novel triazolyl-isatin hybrids, J Enzyme Inhib Med Chem. 31 (2016) 1520–1526. https://doi.org/10.3109/14756366.2016.1151015.

[44] C.R. Prakash, S. Raja, G. Saravanan, Design and synthesis of 4-(1-(4-chlorobenzyl)-2,3-dioxoindolin-5-yl)-1-(4-substituted/unsubstituted benzylidene) semicarbazide: Novel agents with analgesic, anti-inflammatory and ulcerogenic properties, Chinese Chemical Letters. 23 (2012) 541–544. https://doi.org/10.1016/j.cclet.2012.03.014.

[45] A. Medvedev, N. Igosheva, M. Crumeyrolle-Arias, V. Glover, Isatin: Role in stress and anxiety, Stress. 8 (2005) 175–183. https://doi.org/10.1080/10253890500342321.

[46] A.N. Abdalla, M. di Stefano, G. Poli, T. Tuccinardi, A. Bader, A. Vassallo, M.E. Abdallah, M.Z. El-Readi, B. Refaat, A.S. Algarni, R. Ahmad, H.M. Alkahtani, A.A.-M. Abdel-Aziz, A.S. El-Azab, A. Alqathama, Co-Inhibition of P-gp and Hsp90 by an Isatin-Derived Compound Contributes to the Increase of the Chemosensitivity of MCF7/ADR-Resistant Cells to Doxorubicin, Molecules. 27 (2021) 90. https://doi.org/10.3390/molecules27010090.

[47] T. Al-Warhi, D.M. Elimam, Z.M. Elsayed, M.M. Abdel-Aziz, R.M. Maklad, A.A. Al-Karmalawy, K. Afarinkia, M.A.S. Abourehab, H.A. Abdel-Aziz, W.M. Eldehna, Development of novel isatin

thiazolyl-pyrazoline hybrids as promising antimicrobials in MDR pathogens, RSC Adv. 12 (2022) 31466–31477. https://doi.org/10.1039/D2RA04385H.

[48] M. Chuma, K. Terashita, N. Sakamoto, New molecularly targeted therapies against advanced hepatocellular carcinoma: From molecular pathogenesis to clinical trials and future directions, Hepatology Research. 45 (2015) E1–E11. https://doi.org/10.1111/hepr.12459.

[49] A. Morabito, E. de Maio, M. di Maio, N. Normanno, F. Perrone, Tyrosine Kinase Inhibitors of Vascular Endothelial Growth Factor Receptors in Clinical Trials: Current Status and Future Directions, Oncologist. 11 (2006) 753–764. https://doi.org/10.1634/theoncologist.11-7-753.

[50] F. Ahmed, M. Al-Oteibi, S. Layati, F. Kadi, A. Chaudhary, M. Gari, M. Al-Qahtani, Sunitinib effectively reduces clonogenic acute myeloid leukemia cells in vitro, BMC Genomics. 15 (2014) 67–68. https://doi.org/10.1186/1471-2164-15-S2-P67.

[51] W. Fiedler, S. Kayser, M. Kebenko, M. Janning, J. Krauter, M. Schittenhelm, K. Götze, D. Weber, G. Göhring, V. Teleanu, F. Thol, M. Heuser, K. Döhner, A. Ganser, H. Döhner, R.F. Schlenk, A phase I/II study of sunitinib and intensive chemotherapy in patients over 60 years of age with acute myeloid leukaemia and activating *FLT3* mutations, Br J Haematol. 169 (2015) 694–700. https://doi.org/10.1111/bjh.13353.

[52] K. Gowda, C. Annageldiyev, D. Desai, S. Amin, D. Claxton, A. Sharma, Abstract 795: Isatin analog for the treatment of acute myeloid leukemia, Cancer Res. 78 (2018) 795–795. https://doi.org/10.1158/1538-7445.AM2018-795.

[53] N. Mulet-Margalef, X. Garcia del Muro, Sunitinib in the treatment of gastrointestinal stromal tumor: patient selection and perspectives, Onco Targets Ther. Volume 9 (2016) 7573–7582. https://doi.org/10.2147/OTT.S101385.

[54] M. Rizzo, C. Porta, Sunitinib in the treatment of renal cell carcinoma: an update on recent evidence, Ther Adv Urol. 9 (2017) 195–207. https://doi.org/10.1177/1756287217713902.

[55] Z. Ding, M. Zhou, C. Zeng, Recent advances in isatin hybrids as potential anticancer agents, Arch Pharm (Weinheim). 353 (2020) 1900367. https://doi.org/10.1002/ardp.201900367.

[56] M.S. Fenton, K.M. Marion, A.K. Salem, R. Hogen, F. Naeim, J.M. Hershman, Sunitinib Inhibits MEK/ERK and SAPK/JNK Pathways and Increases Sodium/Iodide Symporter Expression in Papillary Thyroid Cancer, Thyroid. 20 (2010) 965–974. https://doi.org/10.1089/thy.2010.0008.

[57] A. Medvedev, O. Buneeva, O. Gnedenko, P. Ershov, A. Ivanov, Isatin, an endogenous nonpeptide biofactor: A review of its molecular targets, mechanisms of actions, and their biomedical implications, BioFactors. 44 (2018) 95–108. https://doi.org/10.1002/biof.1408.

[58] S.N. Singh, S. Regati, A.K. Paul, M. Layek, S. Jayaprakash, K.V. Reddy, G.S. Deora, S. Mukherjee, M. Pal, Cu-mediated 1,3-dipolar cycloaddition of azomethine ylides with dipolarophiles: a faster access to spirooxindoles of potential pharmacological interest, Tetrahedron Lett. 54 (2013) 5448–5452. https://doi.org/10.1016/j.tetlet.2013.07.126.

[59] U. Das, R. Sharma, J. Dimmock, 1,5-Diaryl-3-oxo-1,4-pentadienes: A Case for Antineoplastics with Multiple Targets, Curr Med Chem. 16 (2009) 2001–2020. https://doi.org/10.2174/092986709788682218.

[60] D. Jandial, C. Blair, S. Zhang, L. Krill, Y.-B. Zhang, X. Zi, Molecular Targeted Approaches to Cancer Therapy and Prevention Using Chalcones, Curr Cancer Drug Targets. 14 (2014) 181–200. https://doi.org/10.2174/1568009614666140122160515.

[61] M. Hossain, U. Das, J.R. Dimmock, Recent advances in α,β-unsaturated carbonyl compounds as mitochondrial toxins, Eur J Med Chem. 183 (2019) 111687. https://doi.org/10.1016/j.ejmech.2019.111687.

[62] M. Hossain, U. Das, N. Umemura, H. Sakagami, J. Balzarini, E. de Clercq, M. Kawase, J.R. Dimmock, Tumour-specific cytotoxicity and structure–activity relationships of novel 1-[3-(2-methoxyethylthio)propionyl]-3,5-bis(benzylidene)-4-piperidones, Bioorg Med Chem. 24 (2016) 2206–2214. https://doi.org/10.1016/j.bmc.2016.03.056.

[63] B. Mutus, J.D. Wagner, C.J. Talpas, J.R. Dimmock, O.A. Phillips, R.S. Reid, 1-p-Chlorophenyl-4,4-dimethyl-5-diethylamino-1-penten-3-one hydrobromide, a sulfhydryl-specific compound which reacts irreversibly with protein thiols but reversibly with small molecular weight thiols, Anal Biochem. 177 (1989) 237–243. https://doi.org/10.1016/0003-2697(89)90045-6.

[64] J. Raffel, A.K. Bhattacharyya, A. Gallegos, H. Cui, J.G. Einspahr, D.S. Alberts, G. Powis, Increased expression of thioredoxin-1 in human colorectal cancer is associated with decreased patient survival, Journal of Laboratory and Clinical Medicine. 142 (2003) 46–51. https://doi.org/10.1016/S0022-2143(03)00068-4.

[65] K.J. Cullen, K.A. Newkirk, L.M. Schumaker, N. Aldosari, J.D. Rone, B.R. Haddad, Glutathione S-transferase pi amplification is associated with cisplatin resistance in head and neck squamous cell carcinoma cell lines and primary tumors., Cancer Res. 63 (2003) 8097–102.

[66] J.R. Dimmock, D.W. Elias, M.A. Beazely, N.M. Kandepu, Bioactivities of chalcones., Curr Med Chem. 6 (1999) 1125–49.

[67] R.J. Motzer, B. Escudier, A. Gannon, R.A. Figlin, Sunitinib: Ten Years of Successful Clinical Use and Study in Advanced Renal Cell Carcinoma, Oncologist. 22 (2017) 41–52. https://doi.org/10.1634/THEONCOLOGIST.2016-0197.

[68] M. McTigue, B.W. Murray, J.H. Chen, Y.L. Deng, J. Solowiej, R.S. Kania, Molecular conformations, interactions, and properties associated with drug efficiency and clinical performance among VEGFR TK inhibitors, Proc Natl Acad Sci U S A. 109 (2012) 18281–18289. https://doi.org/10.1073/PNAS.1207759109.

[69] NCI-60 Screening Methodology | NCI-60 Human Tumor Cell Lines Screen | Discovery & Development Services | Developmental Therapeutics Program (DTP), (n.d.). https://dtp.cancer.gov/discovery_development/nci-60/methodology.htm (accessed December 18, 2022).

[70] N.N. Danial, S.J. Korsmeyer, Cell Death: Critical Control Points, Cell. 116 (2004) 205–219. https://doi.org/10.1016/S0092-8674(04)00046-7.

[71] M. Hassan, H. Watari, A. Abualmaaty, Y. Ohba, N. Sakuragi, Apoptosis and molecular targeting therapy in cancer, Biomed Res Int. 2014 (2014). https://doi.org/10.1155/2014/150845.

[72] J. Lopez, S.W.G. Tait, Mitochondrial apoptosis: killing cancer using the enemy within, Br J Cancer. 112 (2015) 957–962. https://doi.org/10.1038/BJC.2015.85.

[73] C.M. Pfeffer, A.T.K. Singh, Apoptosis: A Target for Anticancer Therapy, Int J Mol Sci. 19 (2018). https://doi.org/10.3390/IJMS19020448.

[74] H.K. Matthews, C. Bertoli, R.A.M. de Bruin, Cell cycle control in cancer, Nat Rev Mol Cell Biol. 23 (2022) 74–88. https://doi.org/10.1038/S41580-021-00404-3.

[75] SwissTargetPrediction, (n.d.). http://www.swisstargetprediction.ch/ (accessed December 18, 2022).

[76] A. Daina, O. Michielin, V. Zoete, SwissTargetPrediction: updated data and new features for efficient prediction of protein targets of small molecules, Nucleic Acids Res. 47 (2019) W357–W3664. https://doi.org/10.1093/NAR/GKZ382.

[77] E.J. Morris, S. Jha, C.R. Restaino, P. Dayananth, H. Zhu, A. Cooper, D. Carr, Y. Deng, W. Jin, S. Black, B. Long, J. Liu, E. DiNunzio, W. Windsor, R. Zhang, S. Zhao, M.H. Angagaw, E.M. Pinheiro, J. Desai, L. Xiao, G. Shipps, A. Hruza, J. Wang, J. Kelly, S. Paliwal, X. Gao, B.S. Babu, L. Zhu, P. Daublain, L. Zhang, B.A. Lutterbach, M.R. Pelletier, U. Philippar, P. Siliphaivanh, D. Witter, P. Kirschmeier, W. Robert Bishop, D. Hicklin, D. Gary Gillil, L. Jayaraman, L. Zawel, S. Fawell, A.A. Samatar, Discovery of a novel ERK inhibitor with activity in models of acquired resistance to BRAF and MEK inhibitors, Cancer Discov. 3 (2013) 742–750. https://doi.org/10.1158/2159-8290.CD-13-0070.

[78] RCSB PDB - 6GDM: Fragment-based discovery of a highly potent, orally bioavailable inhibitor which modulates the phosphorylation and catalytic activity of ERK1/2, (n.d.). https://www.rcsb.org/structure/6GDM (accessed December 18, 2022).

[79] A. Daina, O. Michielin, V. Zoete, SwissADME: a free web tool to evaluate pharmacokinetics, drug-likeness and medicinal chemistry friendliness of small molecules, Scientific Reports 2017 7:1. 7 (2017) 1–13. https://doi.org/10.1038/srep42717.

[80] A. Daina, V. Zoete, A BOILED-Egg To Predict Gastrointestinal Absorption and Brain Penetration of Small Molecules, ChemMedChem. 11 (2016) 1117–1121. https://doi.org/10.1002/CMDC.201600182.

[81] Q.-S. Yu, H.-R. Xin, R.-L. Qiu, Z.-L. Deng, F. Deng, Z.-J. Yan, Niclosamide: drug repurposing for human chondrosarcoma treatment via the caspase-dependent mitochondrial apoptotic pathway, Am J Transl Res. 12 (2020) 3688. /pmc/articles/PMC7407720/ (accessed December 18, 2022).

[82] R.D. Pearson, E.L. Hewlett, Niclosamide therapy for tapeworm infections, Ann Intern Med. 102 (1985) 550–551. https://doi.org/10.7326/0003-4819-102-4-550.

[83] H.D. Chae, N. Cox, G. v. Dahl, N.J. Lacayo, K.L. Davis, S. Capolicchio, M. Smith, K.M. Sakamoto, Niclosamide suppresses acute myeloid leukemia cell proliferation through inhibition of CREB-dependent signaling pathways, Oncotarget. 9 (2017) 4301–4317. https://doi.org/10.18632/ONCOTARGET.23794.

[84] J. Gyamfi, Y.H. Lee, B.S. Min, J. Choi, Niclosamide reverses adipocyte induced epithelial-mesenchymal transition in breast cancer cells via suppression of the interleukin-6/STAT3 signalling axis, Sci Rep. 9 (2019). https://doi.org/10.1038/S41598-019-47707-2.

[85] S.Y. Park, J.Y. Kim, J.H. Choi, J.H. Kim, C.J. Lee, P. Singh, S. Sarkar, J.H. Baek, J.S. Nam, Inhibition of LEF1-Mediated DCLK1 by Niclosamide Attenuates Colorectal Cancer Stemness, Clin Cancer Res. 25 (2019) 1415–1429. https://doi.org/10.1158/1078-0432.CCR-18-1232.

[86] Y. Li, P.K. Li, M.J. Roberts, R.C. Arend, R.S. Samant, D.J. Buchsbaum, Multi-targeted therapy of cancer by niclosamide: A new application for an old drug, Cancer Lett. 349 (2014) 8–14. https://doi.org/10.1016/J.CANLET.2014.04.003.

[87] X. Pei, F. Zheng, Y. Li, Z. Lin, X. Han, Y. Feng, Z. Tian, D. Ren, K. Cao, C. Li, Niclosamide Ethanolamine Salt Alleviates Idiopathic Pulmonary Fibrosis by Modulating the PI3K-mTORC1 Pathway, Cells. 11 (2022) 346. https://doi.org/10.3390/CELLS11030346/S1.

[88] S. Saxena, G. Samala, J. Renuka, J.P. Sridevi, P. Yogeeswari, D. Sriram, Development of 2-amino-5-phenylthiophene-3-carboxamide derivatives as novel inhibitors of Mycobacterium tuberculosis DNA GyrB domain, Bioorg Med Chem. 23 (2015) 1402–1412. https://doi.org/10.1016/J.BMC.2015.02.032.

[89] S. Nagarajan, A. Ahmed, H. Choo, Y.S. Cho, K.S. Oh, B.H. Lee, K.J. Shin, A.N. Pae, 3D QSAR pharmacophore model based on diverse IKKβ inhibitors, J Mol Model. 17 (2011) 209–218. https://doi.org/10.1007/S00894-010-0714-8.

[90] A.K. Mankan, M.W. Lawless, S.G. Gray, D. Kelleher, R. McManus, NF-κB regulation: the nuclear response, J Cell Mol Med. 13 (2009) 631. https://doi.org/10.1111/J.1582-4934.2009.00632.X.

[91] Y. Liang, Y. Zhou, P. Shen, NF-kappaB and its regulation on the immune system., Cell Mol Immunol. 1 (2004) 343–50.

[92] J.G. Wright, J.W. Christman, The role of nuclear factor kappa B in the pathogenesis of pulmonary diseases: implications for therapy, Am J Respir Med. 2 (2003) 211–219. https://doi.org/10.1007/BF03256650.

[93] J.W. Christman, R.T. Sadikot, T.S. Blackwell, The role of nuclear factor-kappa B in pulmonary diseases, Chest. 117 (2000) 1482–1487. https://doi.org/10.1378/CHEST.117.5.1482.

[94] D. Thakur, O. Taliaferro, M. Atkinson, R. Stoffel, R.S. Guleria, S. Gupta, Inhibition of nuclear factor κB in the lungs protect bleomycin-induced lung fibrosis in mice, Mol Biol Rep. 49 (2022) 3481–3490. https://doi.org/10.1007/S11033-022-07185-8/TABLES/1.

[95] H.I. Ciftci, S.E. Ozturk, T.F.S. Ali, M.O. Radwan, H. Tateishi, R. Koga, Z. Ocak, M. Can, M. Otsuka, M. Fujita, The First Pentacyclic Triterpenoid Gypsogenin Derivative Exhibiting Anti-ABL1 Kinase and Anti-chronic Myelogenous Leukemia Activities, Biol Pharm Bull. 41 (2018) 570–574. https://doi.org/10.1248/BPB.B17-00902.